Lappeenranta University of Technology

LUT School of Energy Systems

Degree Program in Energy Technology

Mikko Tirola

External Insulation of Nuclear Reactor Pressure Vessel to Mitigate Pressurized Thermal Shock

Master's thesis

Examiners: Professor, D. Sc. (Tech) Juhani Hyvärinen

Supervisors: Research Scientist, M. Sc. (Tech) Jani Laine
M. Sc. (Tech) Timo Toppila
M. Sc. (Tech) Sampsa Launiainen

TIIVISTELMÄ

Lappeenrannan teknillinen yliopisto
School of Energy Systems
Energiatekniikan koulutusohjelma

Mikko Tirola

Ydinreaktorin paineastian paineistetun lämpöshokin lieventäminen ulkoisesti eristämällä

Diplomityö

2019

57 sivua, 23 kuvaa, 1 taulukkoa

Työn tarkastajat: Professori Juhani Hyvärinen

Hakusanat: PTS, reaktorin painesäiliö, ulkoinen jäähdytys, eristys

Paineistettu lämpöshokki on ydinvoimalalle vakava uhka, sillä se voi aiheuttaa reaktoripainesäiliön murtumisen ja johtaa säteilyn leviämiseen ympäristöön. Se aiheutuu onnettomuustilanteessa painesäiliön liiallisesta kylmenemisestä samalla kun sen sisällä vallitsee kova paine. Etenkin painesäiliön hitsisaumat ovat alttiita hajoamiselle paineistetun lämpöshokin takia. Eräs tapa suojautua siltä onkin eristää alttiit saumat ulkopuolisella lämpöeristeellä, jolloin syntyvä lämpötilagradientti jää pienemmäksi. Tämän työn tarkoituksena on aikaisempiin tutkimuksiin pohjautuen suunnitella koeohjelma, jolla selvitetään erilaisten eristeratkaisujen toimivuutta. Aikaisemmissa tutkimuksissa käytetty koelaite muodostaa mittausten pohjan. Lisäksi työssä simuloidaan seinämän lämpötilajakauma, joka analysoidaan olemassa olevilla laskentatyökaluilla niiden demonstroimiseksi.

ABSTRACT

Lappeenranta University of Technology
School of Energy Systems
Degree Program in Energy Technology

Mikko Tirola

External Insulation of Nuclear Reactor Pressure Vessel to Mitigate Pressurized Thermal Shock

Master's Thesis

2019

57 pages, 23 figures, 1 table

Examiners: Professor Juhani Hyvärinen

Keywords: PTS, reactor pressure vessel, external cooling, insulation

Pressurized thermal shock is a serious threat to a nuclear power plant, because it can lead to rupturing of the reactor pressure vessel and release of radioactivity to the environment. It is caused by overcooling of the vessel when there is high internal pressure. The weld seams of the vessel are the most vulnerable spots to the pressurized thermal shock. One way to defend against it is to insulate them with an external insulator to dampen the resulting temperature gradient. The purpose of this thesis is to plan a test program to study the behavior of different insulation configurations. Previous studies on the subject are used as a basis and the test facility constructed previously is to be used for the measurements. Also, to demonstrate the existing calculation tools, the temperature profile during an accident is numerically simulated and analysed.

ACKNOWLEDGEMENTS

I want to thank professor Juhani Hyvärinen for his guidance during the writing of this thesis. I also want to my supervisors Jaine Laine, Timo Toppila and Sampsa Launiainen for their support. In addition, a want to express my gratitude to Fortum for providing the funding, and Tatu Hovi for his advice and everything concerning his IHCP Solver – program.

Lappeenranta 3.3.2019

Mikko Tirola

TABLE OF CONTENTS

NOMENCLATURE

A	area	m^2
C_p	heat capacity	J/K
c_p	specific heat capacity	J/kgK
D	diameter	m
F	convective boiling factor	-
g	gravitational acceleration	m/s^2
h	heat transfer coefficient	W/m^2K
k	thermal conductivity	W/mK
L	length	m
$\dot{m}$	mass flow	kg/s
p	pressure	Pa, bar
q	heat flux	W/m^2
S	nucleate boiling suppression factor	-
T	temperature	K, °C
t	time	s
X	local vapor quality	-
x	distance	m

Greek letters

α	thermal diffusivity	m^2/s
β	thermal expansion coefficient	1/K
ε	arbitrarily small value	
λ	heat of vaporization	J/kg
μ	dynamic viscosity	Pa·s
ν	kinematic viscosity	m^2/s
ρ	density	kg/m^3
σ	surface tension	N/m
ϕ	sensitivity coefficient	-

Dimensionless numbers

Bi	Biot number

Fo	Fourier number
Nu	Nusselt number
Pr	Prandtl number
Ra	Rayleigh number
Re	Reynolds number

Subscripts

db	Dittus-Boelter
eff	effective
est	estimated
fz	Forster-Zuber
L	liquid
S	surface
sat	saturation
surf	surface
TP	two-phase
v	vapor
w	wall
∞	coolant, bulk

Abbreviations

NDT	nil-ductility temperature
PTS	pressurized thermal shock
RPV	reactor pressure vessel

1 INTRODUCTION

1.1 Background

For the operation of a nuclear power plant to be safe, the integrity of the reactor pressure vessel must be guaranteed in all accident scenarios, as its failure could lead to massive fuel damage and potentially also a breach in the containment and to a release of high amounts of radiation. One accident type that could lead to this kind of failure is pressurized thermal shock. It is caused by rapid cooling of the vessel as a result of certain accident scenarios, where cold emergency cooling is introduced to the pressure vessel. The combination of rapid cooling and internal pressure may lead to a catastrophic pressure vessel failure, if the vessel has been embrittled by neutron fluence that is ever-present near the reactor. Because this cannot be allowed to happen, measures must be taken to prevent it.

The focus of this thesis is on external cooling. There are many accident scenarios that can lead to internal cooling and it has been studied in the last decades. However, in Loviisa nuclear power plant the reactor cavity will be flooded in many accident scenarios, possibly leading to external overcooling. There is also a weld seam in the pressure vessel near the core of the reactor. It is thus susceptible to relatively high neutron fluence that worsens the embrittlement. Thus, the effort can be concentrated on this vulnerable spot in the vessel. One possible way to mitigate the resulting thermal shock is to insulate the weld. In previous studies some materials were identified as possibly suitable for this purpose.

1.2 Goals and delimitations

In this thesis the purpose is to devise an experiment program to make the necessary measurements to study the heat transfer through insulated pressure vessel wall. The different insulation materials would be tested using the same experimental facility where previous heat transfer tests for uninsulated wall were performed. From these measurements, heat flux and temperature distribution inside the wall will be calculated to be used in strength calculations. The calculations themselves are beyond the scope of this study, even though they are the end purpose of the experiments.

1.3 Structure of thesis

Chapter 2 deals with theory of the pressurized thermal shock. Its causes and effects are discussed along with the ways to deal with it and how it is analyzed. The theoretical basis of heat transfer is discussed in chapters 3. The methods of heat transfer relevant to the case, correlations for calculation of heat transfer coefficients and relevant dimensionless numbers are focused on. Chapter 4 tells how the measurement data is processed to the desired values using numerical methods. Chapter 5 introduces different possible insulation materials and configurations, properties required from those materials and ways to attach the insulation elements to the reactor pressure vessel. In chapter 6 the existing LUT test facility and the necessary changes to it are discussed. A test program to study the insulation configurations is proposed in chapter 7. Chapter 8 is devoted to the simulated test case used to test and demonstrate the calculation tools used. Finally, in chapter 9 conclusions are presented.

2 PRESSURIZED THERMAL SHOCK

Integrity of the reactor pressure vessel (RPV) is highly important for the safe operation of a nuclear power plant, as a large-scale pressure vessel rupture would breach several safety barriers. Reactor fuel would likely not withstand associated mechanical loads. The resulting pressure inside the containment would be higher than design basis, possibly leading to a release of radioactivity. Pressurized thermal shock (PTS) is an important accident type to study, because it can severely disrupt the integrity of a reactor pressure vessel. It stresses the RPV in two ways. First is the thermal shock that is caused by rapid cooling of material. The temperature gradient over the RPV wall causes thermal stresses that may cause pre-existing cracks to propagate. The second way is the pressure inside the RPV, which may cause a rupture as the cracking weakens the integrity of the vessel. There are many different scenarios, which can lead to PTS in a nuclear reactor. Interestingly, as the thermal shock is strongest when the emergency cooling system works as intended (and the cooling water is as cold as possible), conservative assumptions in PTS accident scenarios are in this way the opposite of the conservative assumptions in other accident scenarios. (Byod 2008, 463-464)

2.1 Embrittlement

When material cools, it starts to lose its ductility. After it cools below a certain temperature called nil ductility transition temperature (NDT), it becomes brittle. When manufactured, the vessel steel has high fracture toughness and a low NDT. Thus, it can endure cooling to lower temperatures without crack propagation. However, when the reactor is operational the vessel is subjected to continuous neutron fluence that causes changes in the lattice structure of the steel. These changes make the material more brittle and raise the NDT. In normal operation, when temperature is over 250 °C, this is not a problem. However, during accidents, where the reactor will be cooled by emergency systems, temperature may drop below or near to NDT. Then the vessel loses its toughness causing pre-existing small cracks (which cannot be completely eliminated in any case) to propagate leading to possible catastrophic rupture. (IAEA 2009, 22-23)

Weld seams are the most vulnerable spots of the reactor pressure vessel during a pressurized thermal shock, because they have impurities like copper and phosphorus,

which amplify the neutron embrittlement. In addition, the welds have residual stresses and other defects that may worsen the cracking. Therefore, the welds are the most important part of the pressure vessel to shield from the PTS. Fortunately, they represent only a fraction of the whole pressure vessel wall, so the most vulnerable welds can be identified, and shielding can be designed specifically for them. (IAEA 2010, 22; IAEA 1992, 16)

2.2 PTS analysis process

PTS analysis is performed to demonstrate that the RPV can withstand realistic accident scenarios with conservative assumptions. The analysis is performed in steps, where previous steps provide necessary data for the next step, in the end resulting in an integrity assessment of the pressure vessel. The process is iterative, so results of the latter steps may cause re-evaluation of the previous steps. The steps are: (IAEA 2006, 3-5.)

- Selection of overcooling sequences
- Thermal hydraulic analyses
- Temperature and stress field calculations
- Fracture mechanics calculations
- Integrity assessment.

In the first step, relevant overcooling sequences are selected for analysis. The goal is to identify and select those accident scenarios, that are PTS events in themselves or that can lead to PTS in some situations. The selection should be made in a comprehensive way and all relevant data and plant specific features should be considered. Probabilistic risk assessment may be used to help identifying the scenarios that are most significant for the total PTS risk. (IAEA 2010, 9.)

The next step is the thermal hydraulic analyses. They are done to aid the transient selection process, as the overcooling transients are complex and thermal hydraulic analyses are needed to identify the limiting events, and to produce input data for later temperature and stress field calculations. These input values include downcomer temperature field, heat transfer coefficients between the wall and the coolant and primary circuit pressure. (IAEA 2006, 14.)

Temperature and stress field calculations are performed to assess the stresses that the RPV wall experiences during the selected transients. Temperature fields, and by extension thermal loads, are calculated. Local conditions like cold plumes must be taken into account. Stresses and strains are normally calculated using advanced numerical methods. In addition to internal pressure and thermal stresses, the residual stresses of cladding and weld must also be considered. (IAEA 2010, 20-21.)

Fracture mechanics calculations are used to evaluate the RPV integrity against a brittle failure. This is done using linear elastic fracture mechanics and stress intensity factor K_I. In more complex cases, elastic-plastic fracture mechanics need to be used. Finite element method is usually recommended for the calculation. (IAEA 2006, 16-17.)

The last step in the PTS analysis procedure is the integrity assessment. In this step, the results from previous steps, like the stress intensity factor, are evaluated for all the transients, safety factors are assessed, and different sources of uncertainty, like material properties and operator actions, are considered and, if necessary, sensitivity studies are performed. (IAEA 2006, 20-23.)

2.3 PTS in Loviisa power plant

In deterministic thermal hydraulic analysis that has been done in Loviisa nuclear power plant, the sequences analyzed have been chosen using the following criteria: (Junninen 2011a, 2-3; Žemulis 2009.).

- Probability of occurrence
- Probability that a cold plume forms in the downcomer
- Repressurization of the primary circuit
- Primary circuit cooling rate
- The final temperature of the primary circuit.

Most of the accident sequences deal with internal cooling. Multiple scenarios can cause internal cooling of the reactor pressure vessel. In some of these scenarios, if the natural circulation in the primary circuit is small, the water in cold legs may become thermally stratified, allowing the very cold emergency cooling water to flow into the RPV without

mixing with warmer water and forming a cold plume in the downcomer. This could happen, for example, if there was a small break in the hot leg. (Junninen 2011a, 8.)

In Loviisa power plant, the reactor cavity will be flooded in most accident scenarios, making external thermal shock a credible threat. The largest temperature gradient happens, when the containment spray (TQ-system) is accidentally activated during a full power operation. Water flooding the cavity would have a temperature of approximately 25 °C and the wall 260 °C. The temperature gradient will be steepest near the outer (cooled) surface of the wall, so any cracks there are most vulnerable to propagation. Fortunately, it is also farthest away from the reactor core and thus receives the smallest neutron fluence, so the embrittling effect is smaller than in other parts of the wall. (Junninen 2011a; IAEA 2006, 40.)

The scenario has been analyzed using APROS-model of the power plant. Reactor is assumed to be in full power, and the primary pressure, temperatures in both hot and cold legs, and coolant mass flow are assumed to be nominal for full power conditions. The transient starts, when the TQ-emergency cooling system is activated by erroneous signal from malfunctioning system. Temperature of the emergency cooling water is around 16 °C. It is assumed that only one TQ-pump in each redundancy is activated, so the water temperature will be the lowest possible. 10 seconds after the initiating signal, reactor is scrammed and the turbines trip. 30 minutes after the beginning, the operator shuts down the TQ-system, which is the only operator action assumed. Figure 1 shows how the water level behaves during the transient. Water starts to flow to the reactor cavity at 740 s, when the water level in steam generator room sump is over 0,4 m. (Junninen 2011b.)

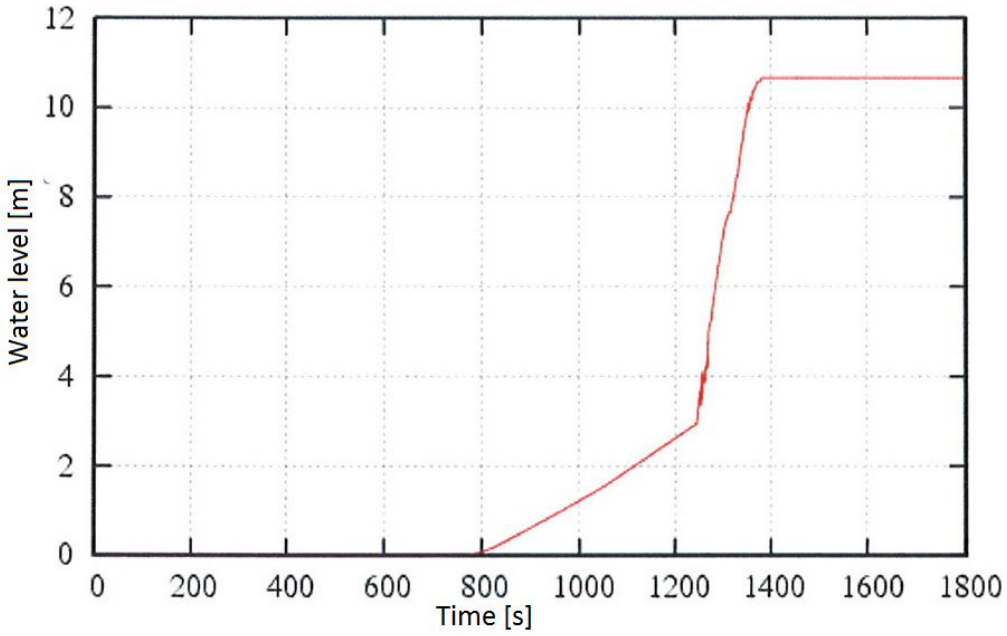

Figure 1: Water level in the reactor cavity. (Junninen 2011b, 14.)

Figure 2 shows how the temperature of RPV weld behaves during the transient. When the water reaches the weld height at around 1300 s, the temperature drops very rapidly.

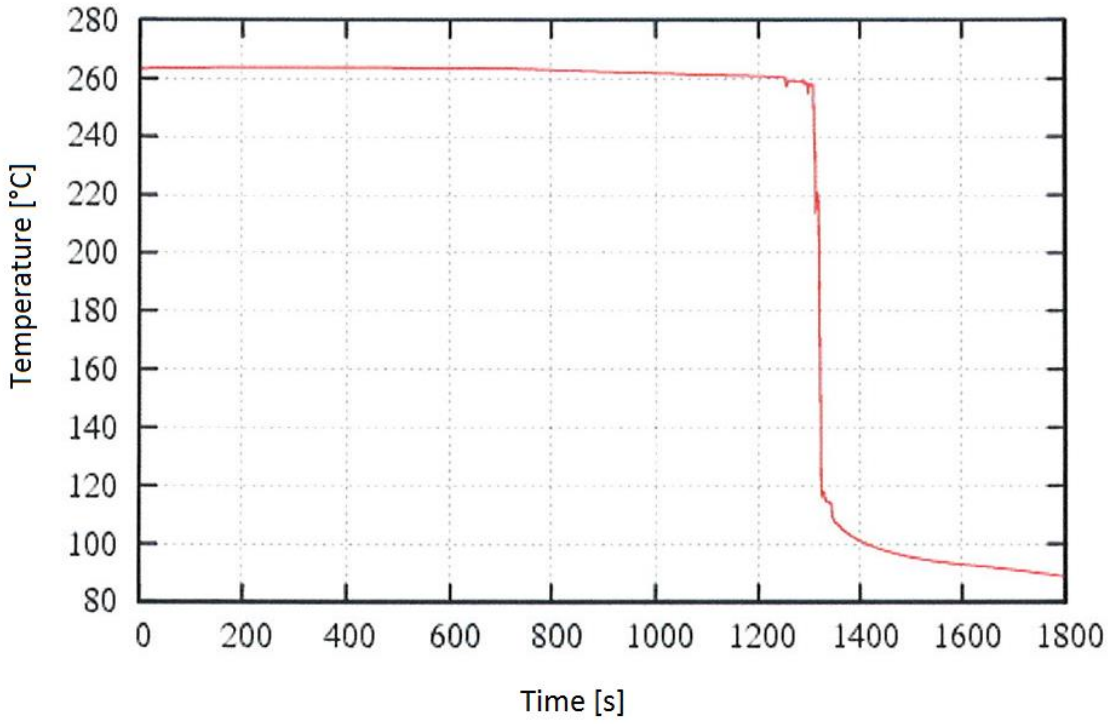

Figure 2: Surface temperature of the RPV weld. (Junninen 2011b, 16.)

The largest heat transfer coefficient during the transient was about 12700 W/m^{2}K and the lowest water temperature at the weld height was 37 °C. The largest heat transfer coefficient corresponds to the waterfront passing the weld when there is intense boiling, that only lasts for a few seconds. (Junninen 2011b, 5.)

2.4 Mitigation of PTS

Risks posed by PTS can be mitigated in various ways. As the neutron flux is the root cause of embrittlement, reducing it by means like low leakage loading patterns, dummy assemblies near the pressure vessel wall or neutron poisons in the periphery are possible. However, they will also reduce the power generated by the reactor. Material properties can also be restored by annealing, as has been done previously in the Loviisa unit 1. That, however, is not a permanent one-off solution, as the material properties start to degrade again when the reactor is in operation. To reduce the mechanical load caused by PTS, temperature of emergency core cooling system water can be raised to some degree, so the thermal shock will not be as severe. As said before, because weld

seams are the most sensitive area of the reactor pressure vessel, one potential way to mitigate the risks of pressurized thermal shock is to dampen the temperature gradient inside the wall by insulating the welds externally from the cold emergency cooling water. In the internal case, thermal insulation would be more difficult to accomplish, as the conditions inside the pressure vessel are harsher than on the outside and it would hinder the flow of the coolant, necessitating a more fundamental redesign of the reactor. How the external insulation could be done is the focus of this study. (IAEA 2010, 49-50; IAEA 2009, 111.)

The goal of the mitigation of PTS is to prevent the combination of low temperature and high stress intensity, where the material is too brittle for prevailing stress conditions causing pre-existing cracks start to propagate. On a one hand the material properties, like fracture toughness, must be good enough during the whole operational life, and on the other hand, the temperature cannot be allowed to become so low that the material becomes too brittle for the stress intensity. This is presented graphically in the figure 3: the blue and the red line must not be allowed to touch. In the real life, as the properties are not known in arbitrary accuracy, there must also be a reasonable margin of error. (IAEA 2010, 3.)

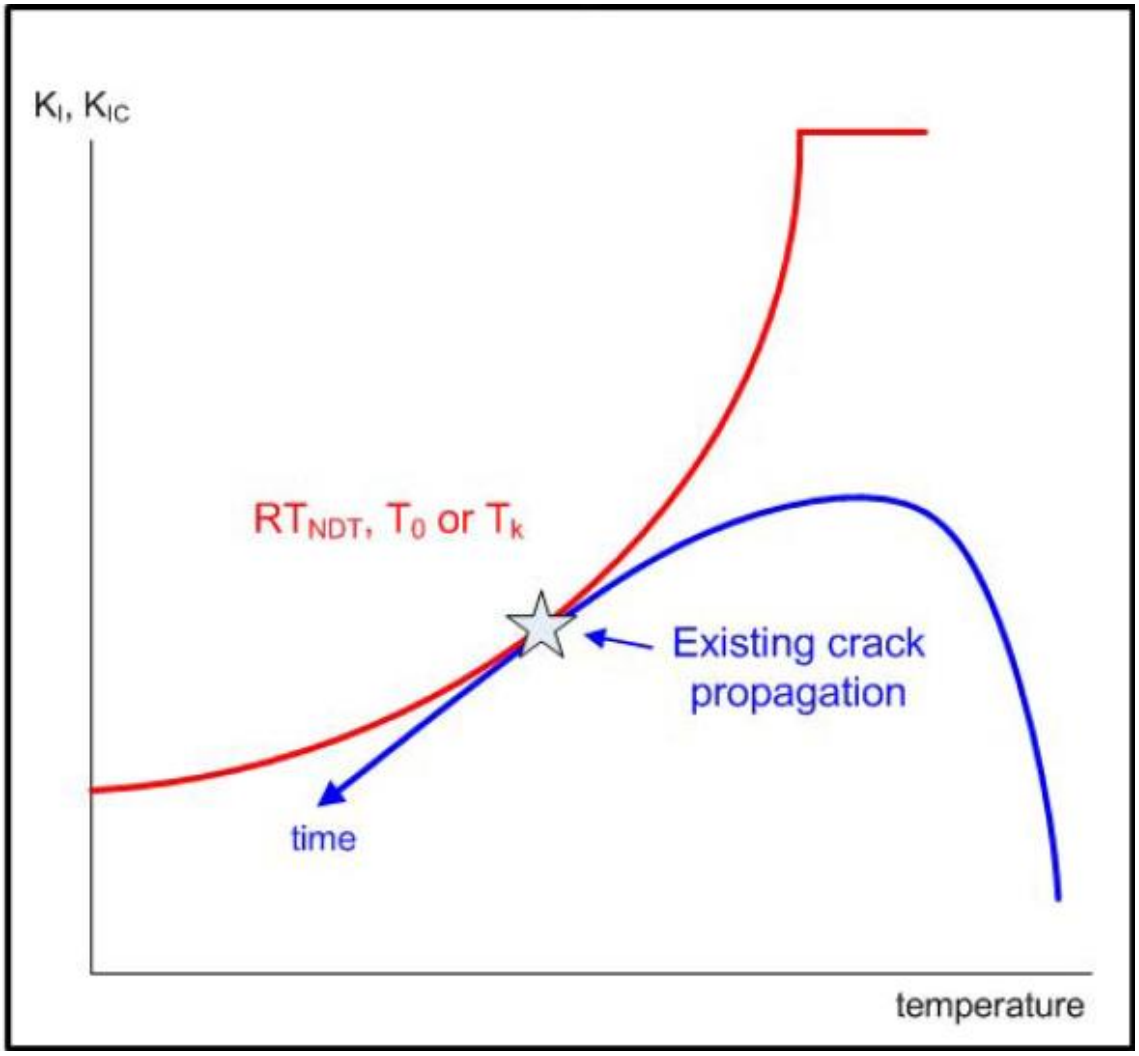

Figure 3: Schematic view of the impact of temperature (horizontal axis) to material fracture toughness. Stress intensity factor is in the vertical axis and the red curve represents the material fracture toughness. The blue curve represents what the material is experiencing. Pre-existing cracks start to propagate, when the stress intensity exceeds the fracture toughness of a given temperature. (IAEA 2010, 4.)

2.5 Previous studies about pressurized thermal shock

Studies about internal pressurized thermal shock have been made since at least the Rancho Seco accident in 1978. In that accident, there was a loss and reapplication of feedwater to the steam generator. Temperature of the cooling water in the hot leg dropped about 180 °C in an hour while the primary-system pressure stayed close to the normal operating pressure. In these studies, most of the prevention measures that were discussed in the previous chapter were suggested. The susceptibility of copper and nickel to neutron fluence was also discovered. (Cheverton 1982, 8-9.)

In general, most of the studies in this area have been about internal cooling accidents, as the embrittlement and therefore cracking is worse in the inner surface of the pressure vessel wall. However, because the reactor cavity in the Loviisa plant will be flooded in several accident scenarios, the external side becomes important as the temperature gradient in these scenarios can be high. (Tuomisto 1997, 210.)

Research on this subject has been done also in Lappeenranta University of Technology. In 2008 a test facility was built to simulate the Loviisa plant pressure vessel wall. Two test series were performed to study and measure heat transfer over the wall in external overcooling situations. This research was continued in 2017, when mitigation of the external PTS by thermally insulating the vulnerable weld was studied. This was done without experiments by creating suitable calculation scripts that were used to simulate different insulation materials and their effect on the pressure vessel wall temperature distribution. (Merisaari 2008; Hovi 2017.)

In this study, the goal is to devise a test program to experimentally measure different insulation configurations. The LUT test facility forms the basis of the tests, and the goal is to measure in real life the different insulation materials, whose properties were studied by computer analysis before. The end goal is to have a test program and the necessary analysis tools to get the temperature distribution inside the measured wall and the heat flux out of the wall when different insulation materials are applied. With these values, stress calculations can be performed, and the plant owners may choose a desired course of action.

3 HEAT TRANSFER

3.1 Heat transfer through RPV Wall

Heat is generated inside the reactor by fission of uranium atoms inside the fuel rods. Rods heat the cooling water surrounding them. Heat is transferred by convection to the reactor pressure vessel wall. For this study, how the heat transfers inside the reactor is not important, as the inside of the wall is assumed to be in a near constant temperature even during accidents. It has been shown, that heat transfer coefficient from the coolant to the downcomer wall is important only when it is less than 3000 – 5000 W/Km^2. When it is higher, the poor thermal conductivity of the stainless steel cladding of the wall is the limiting factor for the heat transfer. (Tuomisto 1997, 210.)

Heat transfer through the pressure vessel wall can be thought as a simple one-dimensional conduction governed by the Fourier's law (equation 1). As the thickness of the insulation layer is small compared to the whole pressure vessel radius the heat transfer in an section of insulation can be handled in Cartesian coordinates. (Incropera et al. 2007, 59.)

$$q_x = -kA\frac{dT}{dx} \tag{1}$$

q_x	Rate of heat flow	[W]
k	Thermal conductivity	[W/m·K]
A	Area	[m^2]
T	Temperature	[K]
x	X-dimensional distance	[m]

This situation is easy to calculate, as the thermal conductivity can be assumed to be constant over the whole wall thickness in the temperature range of the accident. The possible insulation would be placed at the outer edge. Because there is some roughness in the wall and insulation element, a small gap will be left between the wall and the

insulation, which will cause some heat resistance. This contact resistance is not easy to define.

The pressurized thermal shock is a transient phenomenon, where the highest, and the most interesting, heat flux lasts only a couple of seconds when the rising waterfront passes the weld. At first, the water will boil, because the temperature of the wall is so high. During this boiling period, the heat transfer will be highest, and the surface of the wall cools rapidly. In a couple of seconds the wall will be cooled enough for the boiling to end, and the heat flux drops, as convection is not as powerful heat transfer method as boiling. The time of this intense boiling heat transfer can be approximated from the previous measurements conducted in LUT.

Heat transfer from the wall (or insulation) to the cooling water is governed by Newton's law of cooling, presented in equation 2. (Incropera et al. 2007, 350.)

$$q = \bar{h}A(T_S - T_\infty) \tag{2}$$

$\bar{h}$	Average convection coefficient	[W/m^2·K]
T_s	Wall surface temperature	[K]
T_∞	Bulk temperature of water	[K]

Here the convection coefficient is hard to evaluate correctly, because it depends strongly on the dynamic of wall-water interaction, in addition to temperatures involved, flow conditions and whether the water is boiling or not. The flow will go through different boiling regimes rapidly, when it passes the weld. When water is not boiling, heat transfer will happen mostly due to forced convection. Necessary steps to obtain the coefficient using correlations are discussed in chapter 3.2.

To compare the resistances of conduction (inside of the pressure vessel wall) and conduction (from the wall to water), Biot number is used (equation 16). When the number is lower than one, heat transfer inside the wall is dominating, so the wall is in a more uniform temperature during a transient. When the number is higher than one, conduction to the water is dominating and the temperature gradient inside the wall becomes steeper. During the pressurized thermal shock, the Biot number of the wall is

basically always well over one, as the convection coefficient from the wall to water is so high. This holds true even in the beginning of the transient, when the characteristic length can be assumed to be small, as the temperature effect has not penetrated deep to the wall. Therefore, a large temperature gradient will be formed inside the wall. Progression of the temperature profile of the wall and insulation is presented qualitatively in figure 4.

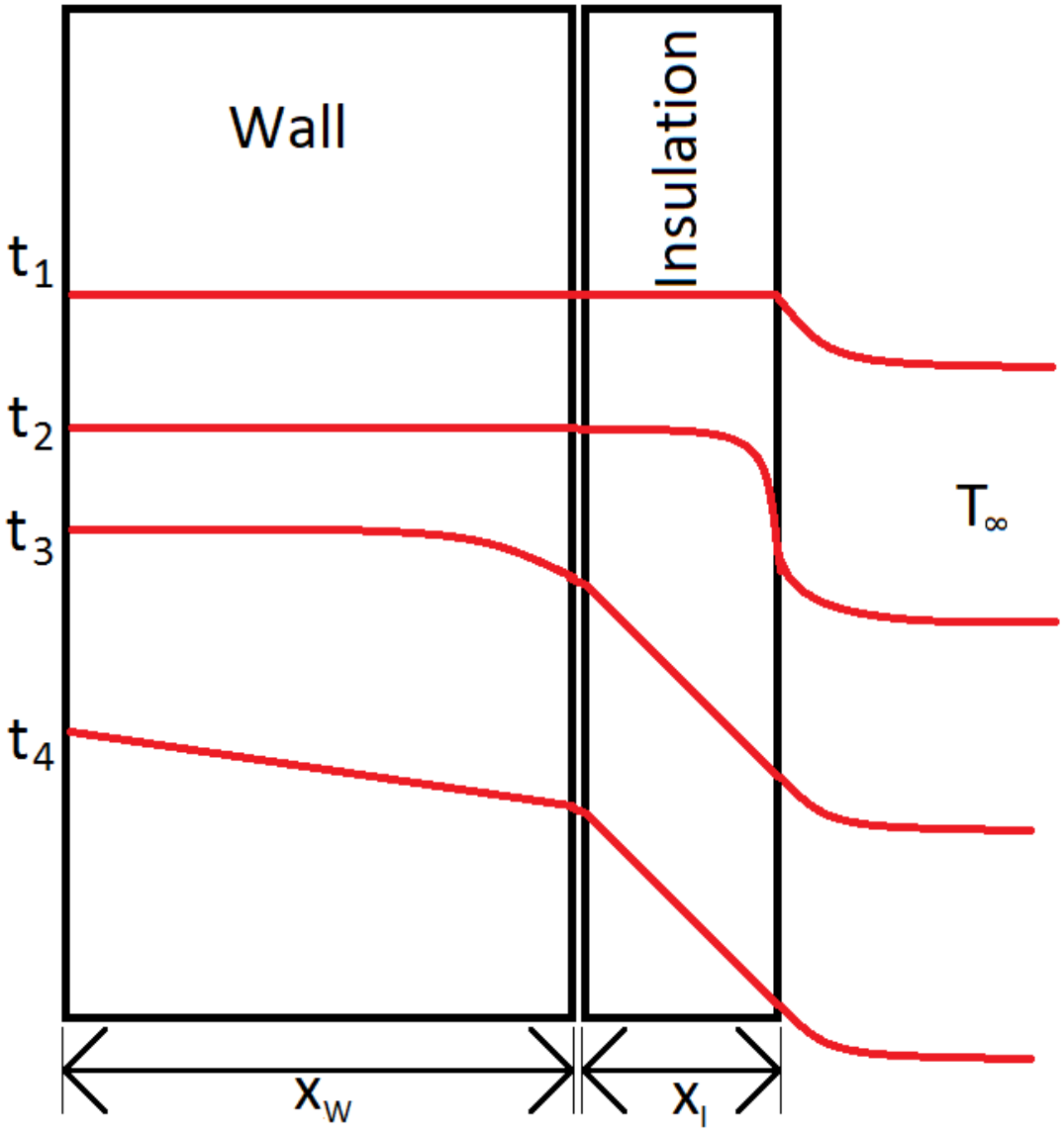

Figure 4: Qualitative temperature distributions of the wall-insulation-system at different times. At time t_1 the wall is in normal operation conditions, and the temperature distribution is nearly uniform. At t_2 the water is rising and boiling happens on the surface. There is a large temperature gradient in the insulation

near the surface. At t_3 the boiling is over and the gradient starts to flatten. At t_4 the system has reached a new steady-state.

3.2 Heat transfer correlations

Convection heat transfer coefficient is parameter that describes the magnitude of heat transfer in convection cases. As it is highly dependent on geometry, flow conditions and other thermodynamic properties, solving it can be a complex task. Many different correlations have been developed to solve the coefficient in different situations. There is not, however, a general correlation that would work in all or even in most cases, so different correlations are needed for different cases. (Incropera et al. 2007, 8.)

Dittus-Boelter correlation (equation 3) is widely used forced convection heat transfer correlation for a flow inside a duct. (Incropera et al. 2007, 514.)

$$Nu_D = 0{,}023 Re_D^{4/5} Pr^n \tag{3}$$

n 0,4 when the fluid is heating and 0,3 when the fluid is cooling

The correlation is valid in the following conditions:

$$\begin{bmatrix} 0{,}7 \leq Pr \leq 160 \\ Re \geq 10000 \\ \frac{L}{D} \geq 10 \end{bmatrix}$$

L Length of a duct [m]

D Diameter of a duct [m]

However, the Dittus-Boelter correlation is for forced convection, and it does not take boiling into account. To take them both into account, Chen correlation can be used.

Chen correlation is a correlation for calculation of convective heat transfer coefficient in saturated two-phase fluid in convective flow, when the heat flux is less than critical flux. (Chen, 1966)

In Chen correlation, total heat transfer coefficient is calculated in two parts as presented in equation 4.

$$h_{total} = Sh_{fz} - Fh_{db} \tag{4}$$

The heat transfer coefficients calculated by Dittus-Boelter (h_{db}) correlation and Forster-Zuber (h_{fz}) correlation are used to represent macroscopic and microscopic scales of heat transfer respectively. Factors *S* and *F* are suppression factor and Reynolds number factor respectively.

Forster-Zuber correlation for nucleate boiling is:

$$h_{fz} = 0{,}00122\left(\frac{k_L^{0,79} C_{p\,L}^{0,45} \rho_L^{0,49} g^{0,25}}{\sigma^{0,5} \mu_L^{0,29} \lambda^{0,24} \rho_v^{0,24}}\right)(T_w - T_{sat})^{0,24}(p(T_w) - p)^{0,75} \tag{5}$$

Suppression factor *S* according to Chen is:

$$S = \left(\frac{\Delta T_{eff}}{\Delta T_{sat}}\right)^{0,99} \tag{6}$$

ΔT_{eff} Effective superheat [K]

ΔT_{sat} Total superheat of the wall [K]

The heat transfer coefficient can be calculated from the Dittus-Boelter correlation (equation 3) by writing the Nusselt number open and rearranging the terms:

$$h_{db} = 0{,}023 Re_L^{0,8} Pr_L^{0,4}\left(\frac{k_L}{D_h}\right) \tag{7}$$

Liquid Reynolds and Prandtl numbers are calculated by equations 8 and 9.

$$Re_L = \frac{\dot{m}(1-X)D_H}{\mu_L} \tag{8}$$

$$Pr_L = \frac{c_{pL}\mu_L}{k_L} \tag{9}$$

Reynolds number factor *F* is obtained by equation 10.

$$F = \left(\frac{Re_{TP}}{Re_L}\right)^{0,8} \tag{10}$$

Re_{TP} Two-phase Reynolds number

Two-phase Reynolds number is calculated by equation 11. (Chen, 1966)

$$Re_{TP} = \frac{DV_{TP}\rho_L}{\mu_L} \tag{11}$$

V_{TP} Effective two-phase velocity [m/s]

Chen correlation is valid only, if the surface temperature is over saturation temperature and below the critical heat flux temperature. Because temperature will be below saturation temperature after the initial boiling, Chen correlation is not enough. Therefore, Fortum has developed post boiling heat transfer correlation based on experiments done in LUT (Merisaari 2008). It is defined as: (Myllymäki 2008, 2.)

$$h = \begin{cases} h_1, & h_1 = h_{cc} + b \quad when\ T_w < T_{sat}\ and\ h_1 \geq h_2 \\ h_2, & h_2 = a \cdot h_1 \quad when\ T_w < T_{sat}\ and\ h_1 > h_2 \end{cases} \tag{12}$$

h_{cc} Churchill & Chu heat transfer coefficient [W/m^2·K]

Coefficients *a* and *b* are empirical constants defined so that they fit measured curve.

$$a = 9{,}15295 \cdot 10^{-4} \cdot \left(T_{surf} - 100\right)^2 + 0{,}06415 \cdot \left(T_{surf} - 100\right) + 2 \tag{13}$$

$$b = 215$$

Churchill-Chu correlation is defined as: (Churchill & Chu, 1975.)

$$h_{cc} = \frac{k}{L}\left(0{,}825 + \frac{0{,}387 \cdot Ra_L^{\frac{1}{6}}}{\left(1 + \left(\frac{0{,}492}{Pr}\right)^{\frac{9}{16}}\right)^{\frac{8}{27}}}\right)^2 \tag{14}$$

Rayleigh number is defined as (Incropera et al. 2007, 569.)

$$Ra_L = \frac{g\beta(T_w - T_\infty)L^3}{\nu\alpha} \quad (15)$$

3.3 Dimensionless approach

Dimensionless numbers can be used to describe different physical phenomena. For transient convection situations, the most relevant dimensionless numbers are Biot number and Fourier number. The heat transfer properties of different insulation materials can be grouped using these numbers in a simplified way.

3.3.1 Biot number

The Biot number is a dimensionless parameter that measures the relation between thermal resistance (or temperature drop) inside a solid and between the surface of the solid and a fluid. When the number is below one, the heat transfer inside the solid is higher than outside, and if it is small enough, the solid can be assumed to be in a uniform temperature. If the number is larger than one, the conduction from its surface is the dominating factor, and the temperature distribution inside the solid becomes steeper the higher the Biot number is. (Incropera et al. 2007, 261.)

$$Bi = \frac{L_c h}{k} \quad (16)$$

L_c Characteristic length [m]

Characteristic length is the interesting spatial dimension of the solid in question. In the case of insulation, it is the thickness of the insulation material. In the case of the wall, it is not reasonable to use the whole thickness of the wall when only brief transients are of interest, as the heat transfer effect has not penetrated through the whole depth of the wall. In these situations, the characteristic length is the part of the wall, where the temperature has started to change due to the cooling effect.

3.3.2 **Fourier number**

Fourier number is the ratio between heat conduction rate and the rate of thermal energy storage in a solid. It can be described as dimensionless time. Fourier number is calculated using equation 17. (Incropera et al. 2007, 376.)

$$Fo = \frac{\alpha t}{L^2} \tag{17}$$

t Characteristic time [s]

Characteristic time is the duration of the most intense convection i.e. boiling. According to previous experiments in LUT, this is usually couple of seconds. Different Fourier numbers can be calculated to represent the whole range of possibilities.

4 ANALYSIS PROCESS

Experiments will result in temperature measurements. Because the surface temperature of the wall cannot be directly measured, heat flux cannot be calculated directly. Therefore, it must be calculated using inverse calculation. A numeric model is needed. The problem can be thought as time dependent conduction in one dimension. First, the heat equation (equation 18) must be discretized. There is no heat generation, only conduction. (Incropera et al. 2007, 302.)

For one dimensional transient conduction with constant material properties and no internal heat generation, the heat equation has the form of equation 18.

$$\frac{1}{\alpha}\frac{\partial T}{\partial t} = \frac{\partial^2 T}{\partial x^2} \tag{18}$$

This equation is then discretized to finite-difference form. For spatial derivative this is done using central difference approximation. Subscript *n* designates the position of the node in x-direction.

$$\left.\frac{\partial^2 T}{\partial x^2}\right|_n \approx \frac{T_{n+1} + T_{n-1} - 2T_n}{(\Delta x)^2} \tag{19}$$

For the time derivative of the equation 18, the finite-difference form is

$$\left.\frac{\partial T}{\partial t}\right|_n \approx \frac{T_n^{p+1} - T_n^p}{\Delta t} \tag{20}$$

Where superscript *p* describes discretized time, so that

$$t = p\Delta t \tag{21}$$

Δt Size of a time step [s]

In this notation *p* is the current new time and *p*+1 is the next time, that happens Δt afterwards.

The preceding spatial and time derivatives can be combined to form the whole finite-difference equation (equation 22). Implicit scheme is used, so the time derivative of

equation 18 is considered to be a backward-difference approximation. In implicit schemes, the temperatures of a new time step (p+1) depend on other temperatures in the same time step that are unknown. Therefore, temperatures for all nodes must be solved simultaneously using, for example, Gauss-Seidel iteration. Implicit method is unconditionally stable, so Δt can be larger than if explicit method was used, which can save computational time. (Incropera et al. 2007, 310.)

$$\frac{1}{\alpha}\frac{T_n^{p+1} - T_n^p}{\Delta t} = \frac{T_{n+1}^{p+1} + T_{n-1}^{p+1} - 2T_n^{p+1}}{(\Delta x)^2} \tag{22}$$

Thermal diffusivity α is defined as

$$\alpha = \frac{k}{\rho c_p} \tag{23}$$

Combining the previous equations, equations used for each calculation node are:

$$\begin{cases} k\dfrac{T_{heater} - T_n^{p+1}}{2\Delta x} - k\dfrac{T_n^{p+1} - T_{n+1}^{p+1}}{\Delta x} = \rho c_p \dfrac{\Delta x}{2}\dfrac{\left(T_n^{p+1} - T_n^p\right)}{\Delta t}, & n = 1 \\ k\dfrac{T_{n-1}^{p+1} - T_n^{p+1}}{\Delta x} - k\dfrac{T_n^{p+1} - T_{n+1}^{p+1}}{\Delta x} = \rho c_p \Delta x \dfrac{\left(T_n^{p+1} - T_n^p\right)}{\Delta t}, & 2 \le n \le N \\ k\dfrac{T_{n-1}^{p+1} - T_n^{p+1}}{\Delta x} - h\left(T_\infty^{p+1} - T_n^{p+1}\right) = \rho c_p \dfrac{\Delta x}{2}\dfrac{\left(T_n^{p+1} - T_n^p\right)}{\Delta t}, & n = N \end{cases} \tag{24}$$

These equations can be simplified by recalling Biot and Fourier numbers (equations 16 and 17) and rearranging

$$\begin{cases} -FoT_{heater} + (1 + 3Fo)T_n^{p+1} - 2FoT_{n+1}^{p+1} = T_n^p, & n = 1 \\ -FoT_{n-1}^{p+1} + (1 + 2Fo)T_n^{p+1} - FoT_{n+1}^{p+1} = T_n^p, & 2 \le n \le N-1 \\ -2FoT_{n-1}^{p+1} + (1 + 2BiFo + 2Fo)T_n^{p+1} = T_n^p + 2BiFoT_\infty, & n = N \end{cases} \tag{25}$$

In the node in the edge of the wall and the insulation, by using averaged density and specific heat, but material specific thermal conductivities. (Hovi 2017, 44.)

$$k_1\frac{T_{n-1}^{p+1} - T_n^{p+1}}{\Delta x} - k_2\frac{T_n^{p+1} - T_{n+1}^{p+1}}{\Delta x} = \bar{\rho}\bar{c_p}\Delta x\frac{\left(T_n^{p+1} - T_n^p\right)}{\Delta t} \tag{26}$$

$$-\overline{Fo_{n-1}}T_{n-1}^{p+1} + (1 + \overline{Fo_{n-1}} + \overline{Fo_{n+1}})T_n^{p+1} - \overline{Fo_{n+1}}T_{n+1}^{p+1} = T_n^p \quad (27)$$

By naming the constant coefficients before each T_n a_n and the right side of the equations C_n, the equation 25 can be arranged to a matrix form, so that

$$[A][T] = [C] \quad (28)$$

Where $[A]$ is composed all the a_n-coefficients, $[T]$ is the temperature vector and $[C]$ is a constant vector composed of C_ns. The temperatures can be solved, for example, by inverse matrix method.

4.1 Inverse calculation

Inverse heat conduction problem is a problem, where the surface heat flux or temperature histories of a solid must be solved from internal temperature measurements. This is contrasted by direct heat conduction problems, where the temperature distribution inside a solid must be solved from known heat flux or surface temperatures. (Beck et al. 1985, 1.)

To solve heat flux from the known temperature distribution, inverse calculation must be used. First, surface heat flux is guessed, and a corresponding temperature field is calculated. Then, the heat flux is disturbed a little and the new temperature field is solved. From this, sensitivity coefficients can be calculated for each thermocouple location. (Krishnan & Sharma 1996, 207.)

$$\phi = \frac{\partial T}{\partial q''_s} = \frac{T_{est}\left(q''_s(1+\varepsilon)\right) - T_{est}\left(q''_s\right)}{\varepsilon q''_s} \quad (29)$$

ϕ Sensitivity coefficient

ε Arbitrarily small value

With the sensitivity coefficient, the assumed heat flux can be corrected by equations 30 and 31.

$$q''_s = \frac{\sum_{r=1}^{R}(T_{mea} - T_{est})\phi_i}{\sum_{r=1}^{R}(\phi_i)^2} \quad (30)$$

r time step

$$q''_{s,new} = q''_{s,old} + \omega q''_s \quad (31)$$

Calculation is repeated, until the convergence condition is reached. Equation 32 shows the condition.

$$\frac{\Delta q''_s}{q''_{s,new}} \leq 0{,}0005 \quad (32)$$

4.2 IHCP Solver LUT

The program used to calculate heat flux and heat transfer coefficient from the measured temperatures is called Inverse Heat Conduction Problem Solver LUT (IHCP LUT). It is written in Python using Tkinter and SciPy. The program takes measured temperatures and relevant material properties as an input and calculates temperature distribution, heat flux and heat transfer coefficient using inverse calculation. Figure 5 shows the user interface of the program. (Hovi 2018.)

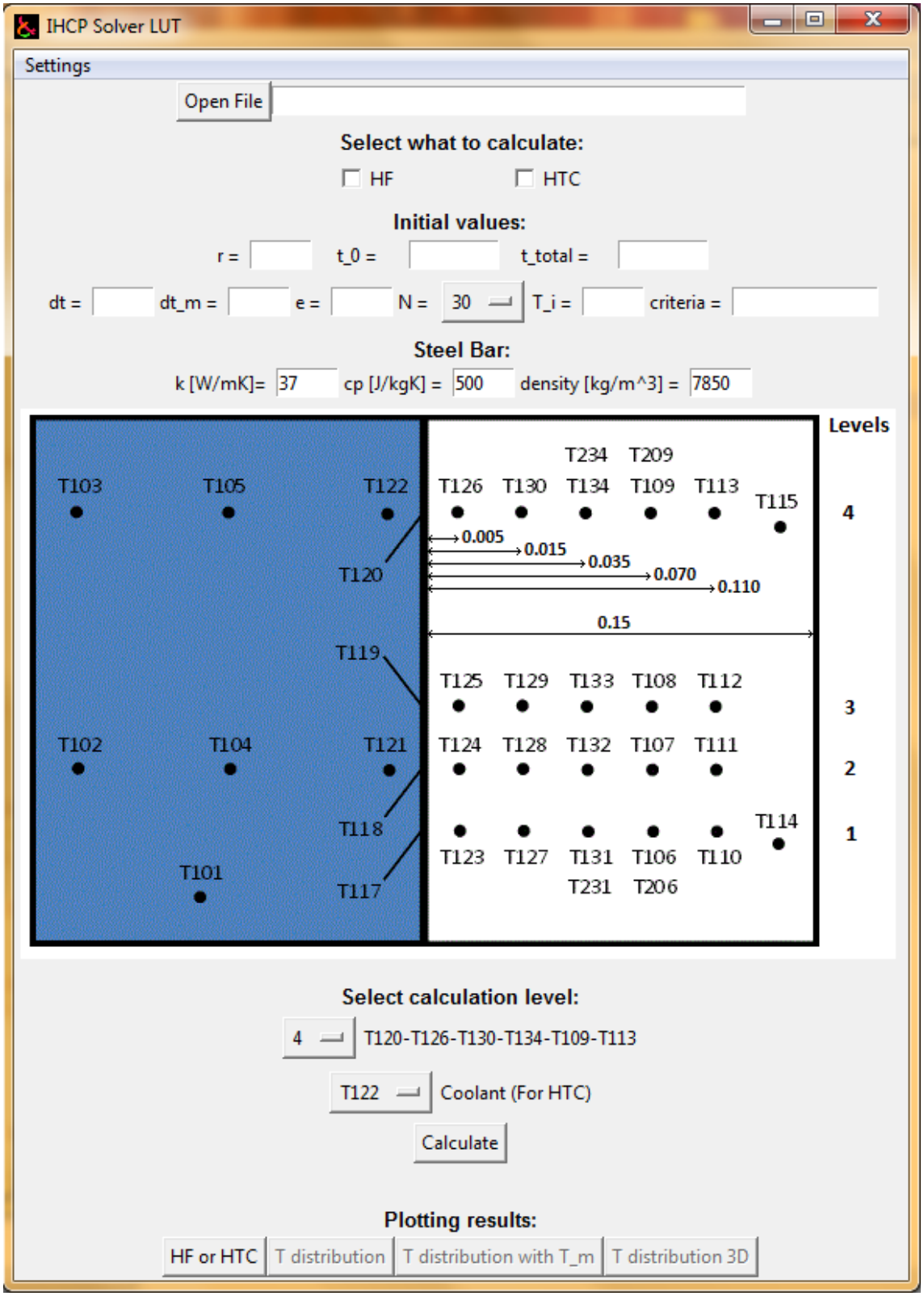

Figure 5: Interface of the program. Temperature measurements are read from a file and other necessary values are fed from this screen. (Hovi 2018.)

5 DIFFERENT INSULATION CONFIGURATIONS

The purpose of the insulation is to lessen the heat transfer between the RPV and the surrounding water during an accident and thus dampen the temperature gradient that forms inside the RPV wall. High peaks of heat transfer rate associated with sudden boiling are dangerous, as they put the wall under much stress, as discussed in chapter 2. The main methods of heat transfer in this case are convection and conduction. The effect of radiation heat transfer can be assumed to be minimal as the temperatures are relatively low. Thermal properties of some possible insulation materials are presented in Appendix I and the properties of the reactor pressure vessel material are presented in Appendix II.

5.1 Required properties

The chosen material should have suitably low thermal conduction and diffusivity. Thermal conductivity defines the rate at which the material transfers thermal energy. As the purpose of the insulator is to slow down the heat transfer process, a low conductivity is desirable. Thermal diffusivity measures how well the material conducts thermal energy relative to its ability to store thermal energy. In practice, this means how fast the material responds to changes of temperature in its environment. A low response speed is beneficial in thermal shock mitigation. (Incropera et al. 2007, 60, 68.)

Whatever the insulation material is, it must be able to withstand the difficult ambient conditions in the reactor cavity. It must resist the neutron fluence and high temperatures near the reactor during normal operation without significant damage. Additionally, it must withstand water and steam during accidents. However, as the purpose of the insulation is to protect the reactor vessel and not itself, it does not need to be able to withstand the accident more than once. It may also be severely damaged in the accident, as long as it is still able to protect the vessel. The most critical time frame is the large initial spike in the heat flux, when the rising water boils on the surface. After the weld seam is completely immersed in the water that is not boiling anymore, the heat transfer should soon be low enough that the vessel is not in danger anymore and the insulation is not needed. Also, it would be beneficial, but not strictly necessary, to have the insulation attached in such a way that it can be removed for inspection of the RPV. The

inspection can be done from the inside, but the insulation must not release anything that would hamper ultrasound inspection. (Toppila & Launiainen, 2018.)

The insulation configuration must withstand different possible situations like startup, shutdown, normal operation and accident scenarios. From the thermal shock point of view, a large-scale loss-of-coolant-accident is not the most limiting case, because the reactor pressure vessel would be cooled also from the inside, making the temperature gradient over the wall less severe than in external-only-cooling cases. However, in severe accidents the RPV is supposed to be cooled from the outside. Therefore, the thermal insulation must be designed so, that the effect does not hinder the desired cooling too much. For this reason, the insulation should not cover more than 30 cm wide section of the RPV. (Ibid.)

5.2 Rejected insulation materials

The insulation material must withstand the challenging conditions that exist in the reactor cavity during normal operation of the reactor and in different accident scenarios. These conditions include high temperature (over 250 °C), neutron fluence and gamma radiation during normal operation, and water, boiling and steam during an accident. Therefore, a number of materials are rejected.

Materials with copper, nickel and phosphorus are susceptible to radiation embrittlement. Even relatively small concentrations (less than 0,3 %) of these elements may increase the susceptibility substantially. For this reason, their presence in the pressure vessel steel must be very limited. An insulation made from these materials may not be sturdy enough for accidents. (IAEA 2009, 12.)

Polytetrafluoroethylene (PTFE, or Teflon) is damaged by radiation quickly, even though it has the necessary temperature resistance and it would be an adequate insulator. (National Aeronautics and Space Administration 1970, 11.)

Phenolic foam, elastomeric foam, polystyrene and polyurethane are all common insulators, but they all have a too low operational temperature. (Engineering ToolBox 2005.)

Paints and adhesives with organic bases, and rubbers are susceptible to radiation damage. (National Aeronautics and Space Administration 1970, 12; Scagliusi et al. 2015, 7.)

Materials, which can release debris causing sump clogging, are problematic in accident scenarios. (Murani 1997.)

5.3 Ceramic materials

Ceramics are non-metallic, inorganic compounds. Some of them are useful in insulation, because they have a low thermal conductivity and other suitable heat transfer properties. They can also resist high temperatures. (The Ceramic Society of Japan. 2012, 3.)

Compared to metals, ceramics are more brittle and have a lower heat transfer coefficient. This makes them more susceptible to thermal shocks, which may limit their usefulness as insulators in pressurized thermal shock situations. (Carter & Norton 2013, 655.)

Possibly useful ceramic materials that were studied previously in LUT are MACOR® and Calcium silicate. Both are highly machinable materials, so making suitable insulator sections should not be a problem.

5.4 Metals

Metals and their alloys are usually good thermal conductors, so to use them for insulation may seem somewhat paradoxical. However, as the insulation needed to shield the reactor pressure vessel is not that much, some metals are adequate for the job. Other thermal properties of metals are suitable for the role, as their melting point is much higher than the about 260 °C present in the reactor cavity.

Another aspect that is relevant to metals is corrosion. When different metals are in electrical contact with each other, there is a risk of galvanic corrosion, where the nobler one of the pair will corrode the less noble metal. An insulator that could corrode the pressure vessel would be unusable. Fortunately, for the electrical contact to be

significant, there needs to be some electrolyte, like water, present. Because the reactor cavity is dry and warm during normal operation, galvanic corrosion should not be a problem during normal operation, and the corrosion effect is not fast enough to have an effect during accidents, when the cavity is flooded. (Papavinasam 2013, 265.)

Possible metallic insulation materials are different steels, titanium alloys or zirconium.

Insulation elements should be easy to make from metals. They would be curved sections small enough to be fitted from the observation hatch at the bottom of the reactor cavity. Magnets could be fitted to the sections for attachment, or some kind of tightening mechanism could be devised.

5.5 Other possibilities

Reflective metallic insulation is in use in nuclear power plants. It is used to insulate primary coolant systems, piping, RPV and other equipment. It is made from elements that can be fastened by buckle belts for easy removal. However, the insulation blocks may well be too large for the reactor cavity and they may hinder the necessary emergency cooling of the reactor too much. (Kolbe & Gahan 1982, A-1.)

Steel wool is another material that could be used for insulation. It can be made from the same steels as the steel insulations discussed in the previous section. It has better insulative properties than plain steel, as there is air inside the material, however when it is wetted the properties change, and they should be studied well before practical solutions are presented. Other similar materials like mineral wool could also be possible if it can be ascertained that they do not release debris that could cause sump clogging. Some encapsulated mineral wool blocks are used in nuclear plants (Kolbe & Gaham 1982, A-2.)

Another insulation possibility would be maze-like insulation. In this concept, there is a geometry (a simple cross-section is presented in figure 6) that would trap steam or air and therefore keep the flooding water in the reactor cavity from directly touching the weld seam. This would prevent boiling in the weld surface lowering the heat flux. This type of solution is highly dependent on flow conditions, so much testing needs to be performed to find an adequate geometry and material.

Figure 6: Simple maze insulation. Steam from the boiling water raising from below fills the cavity and insulate the weld. In real life more complex geometries may be desirable.

5.6 Attachment

Whatever attachment method is used, it needs to be strong enough to withstand the flooding of the reactor cavity and boiling of the water in accident conditions without displacing. It must also be small enough to be installed through the inspection hatches below the reactor cavity using manipulator arms, and it would be good, if it could be removed for inspections of the weld. The last requirement is not absolute, however, as the inspections can also be done from the inside. (Toppila & Launiainen 2018.)

Because the reactor pressure vessel cannot be damaged, no welds or drillings can be made to it. Another unsatisfactory option would be to install the insulation material to the wall of the reactor cavity, and press it to the RPV. That cannot be done, because there is a reflector sheet on the cavity wall that should not be damaged. Realistic attachment options therefore cannot have mechanical installation. One possibility is to use magnets. The insulation could be made from elements, that are small enough to be inserted through the hatches in the bottom of the reactor cavity and they could be then magnetically installed to the pressure vessel wall. Another possibility is to use some

insulation material that can be rolled on the surface and then fasten it mechanically by some wrapping, like a metal foil. This option would be relatively easy to install and take off considering the cramped space in the reactor cavity. (Ibid.)

Because the pressure vessel is not mathematically round and smooth, regardless of the attachment method there will be a small gap between the insulation and the wall. This will cause some contact resistance in the interface which is good from the insulation point of view because it reduces the heat transfer. However, this effect should not be very large, and measurements are needed to study its effects on heat transfer and attachment.

6 LUT TEST FACILITY

6.1 Current status

The test facility was originally constructed to study heat transfer through the reactor pressure vessel walls in the Loviisa nuclear power plant. These original experiments and the configuration of the facility are documented in *Heat transfer experiments for external cooling of a nuclear reactor pressure vessel*. (Merisaari 2008.)

Main component of the test facility is a steel bar, which represents the RPV wall. It is 150 mm thick and made of 10CrMo9-10 steel. In the real plant, pressure vessel walls are 140 mm thick and have additional 9 mm liner. The material was chosen, because its heat transfer properties are similar to the actual RPV wall material 15Cr2MoV. RPV liner is not considered, as its overall effect on the cooling on the outside of the wall is insignificant. The bar is long enough to observe vertical phenomena and wide enough so that heat transfer from sides can be ignored. The test facility is not curved, as the pressure vessel is wide enough for the curvature to be ignored. (Merisaari 2008, 25-30.)

The flow channel is made from steel walls that are 4 mm (sides) and 8 mm (front) thick. Channel has rectangular cross-section: it is 300 mm wide and 100 mm thick (see figure 7). It was designed so, that the velocity distribution is constant. Two windows are installed to allow visual observations. (Ibid.)

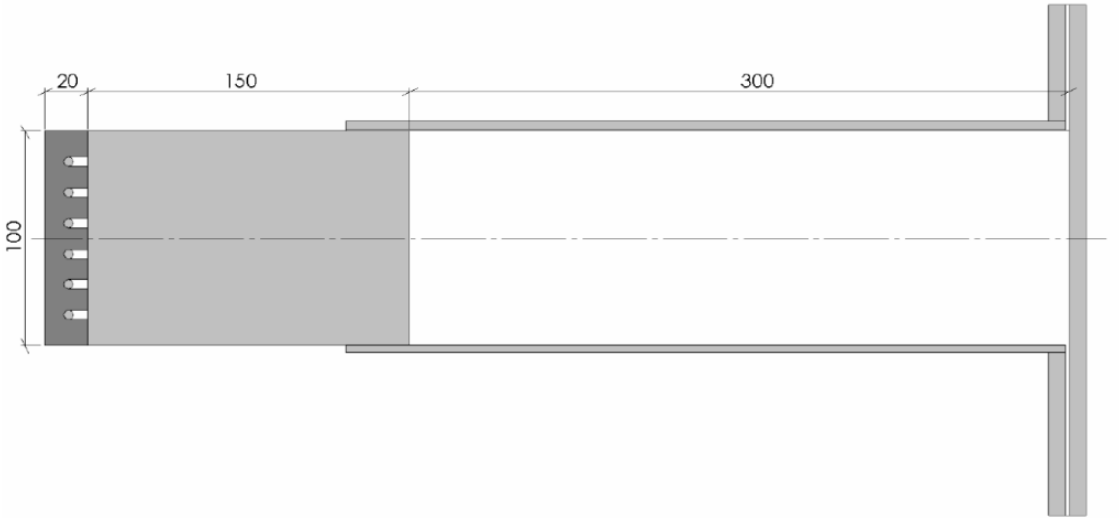

Figure 7: Cross-section of the flow channel (Merisaari 2008, 28.).

To represent the heat generation inside a nuclear reactor, the steel bar is heated from one side to reactor coolant inlet temperature of 260 °C. About 8 kW of heating power was installed to achieve a constant temperature for steady state tests. The heater element was made from six heater rods inside an aluminum plate, which spread the heat evenly. (Ibid.)

26 K-type thermocouples were installed to measure temperature in different points inside the steel bar. In addition, 6 thermocouples measured the temperature of the water inside the flow channel and 2 others were measuring the temperatures of the channel inlet and flow meter. Figure 8 shows the positions of the thermocouples. Water flow rate was measured by a flow meter and the water level by a differential pressure sensor. The complete listing of the measurement instrumentation is presented in Appendix III (Ibid.)

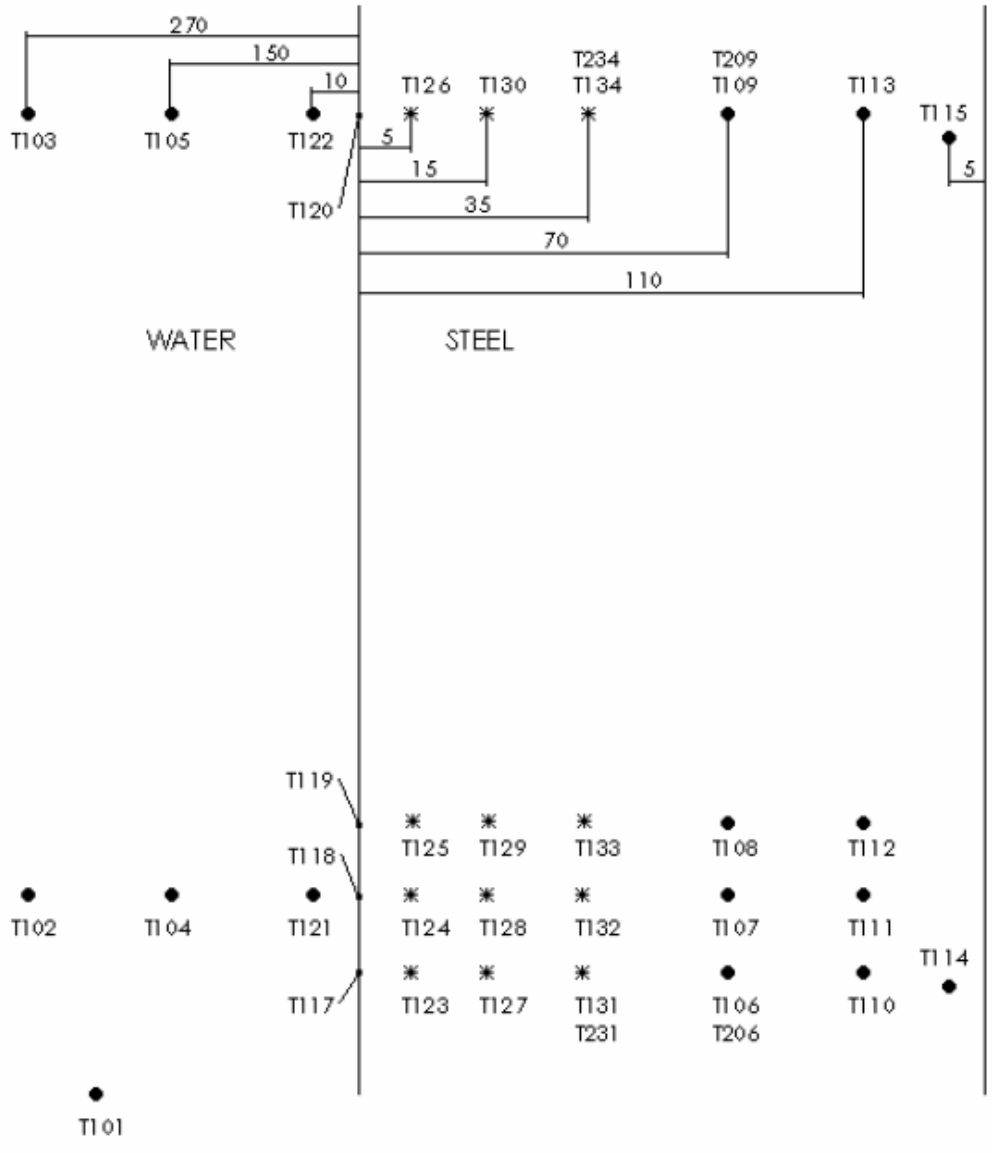

Figure 8: Thermocouple positions in the wall. Figure is not to scale. T206, T209, T231, and T234 are off-centerline thermocouples. (Merisaari 2008, 58.)

6.2 Necessary changes

Recently different studies have been conducted with the test facility, so it has been configured differently. Figure 9 shows the current look of the test facility.

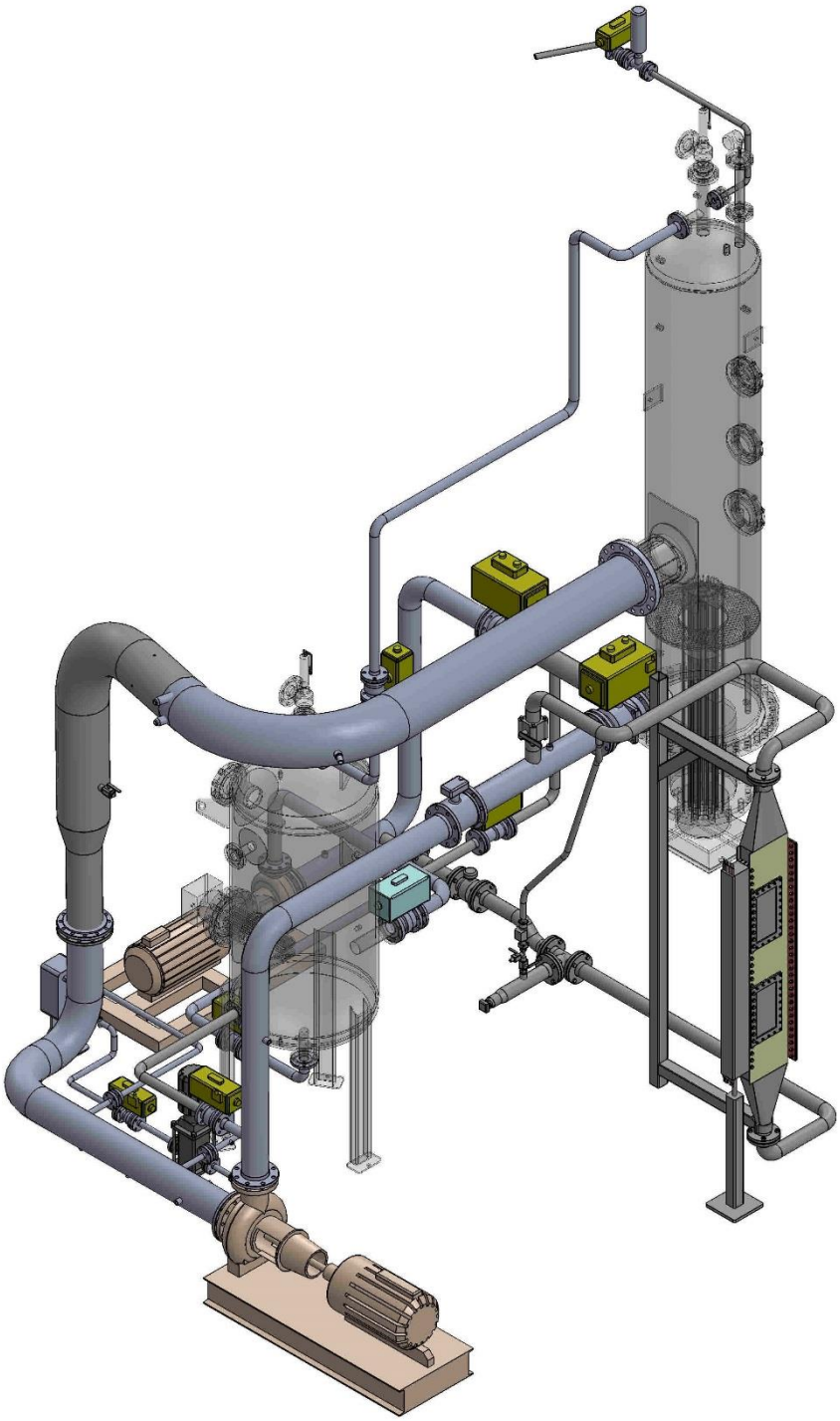

Figure 9: Test facility as it is currently. (Laine 2018.)

In the recent studies the flow direction has been from top-to-bottom. For these measurements, it must be changed back to bottom-to-top. It can be done by changing the orientation of the pump P4 (in figure 10).

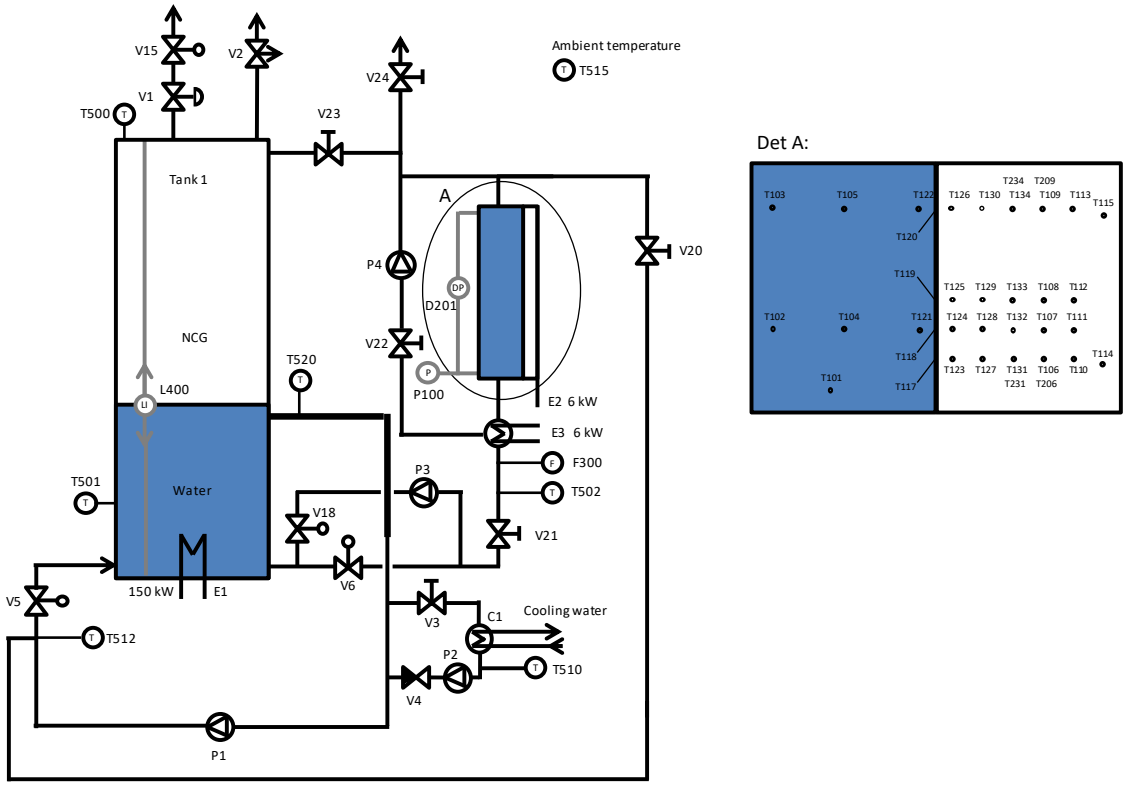

Figure 10: Current flow chart and temperature measurements. (Laine 2018.)

Figure 11 shows the measurement section of the facility. Two more windows have been added since the measurements of 2008 for flow measurements using particle image velocimetry (PIV).

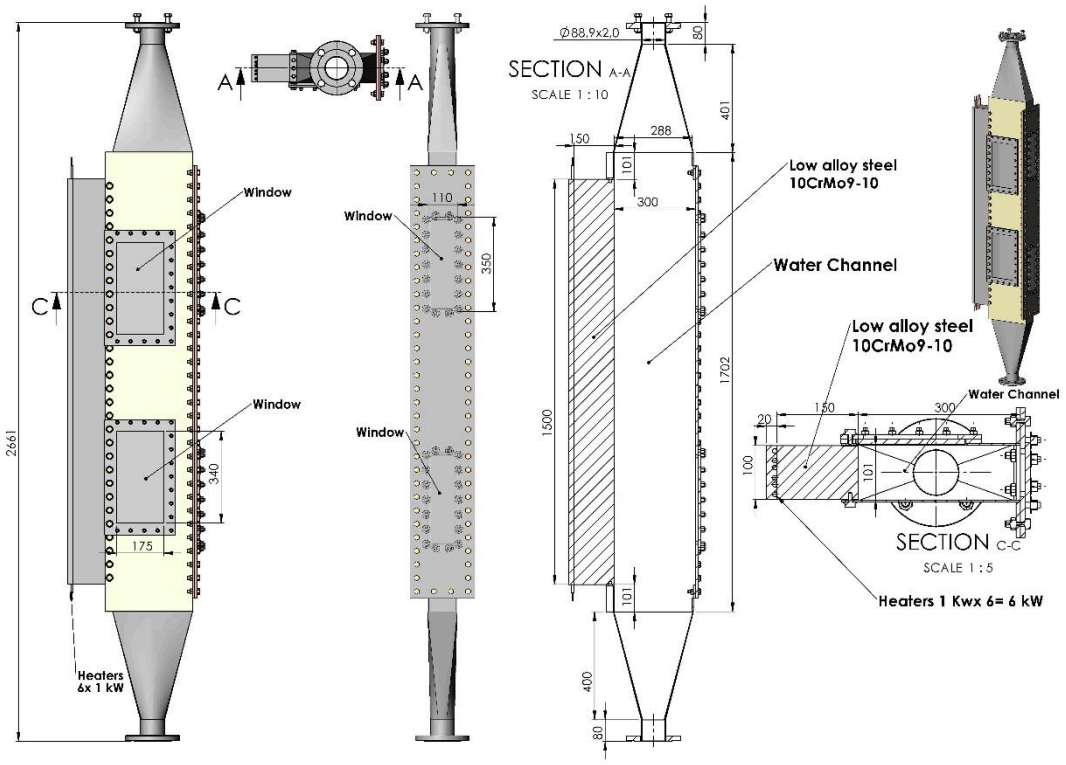

Figure 11: Measurement section of the test facility. (Laine 2018.)

Different insulation configurations can be installed through the observations windows in the test facility wall. Windows are mounted with bolts, so it is relatively easy to take them out of the way and reattach them. If magnetic attachment is used for the insulators, changing them will not be hard. Magnetically attached objects of similar size have been used in other studies with this test facility.

The same measurement sensors that have been used before, can be also used in these measurements. The currently installed k-type thermocouples are sufficient to these measurements and the flow velocities are in range of the current flowmeter (about 2,4 l/s for 8 cm/s rise velocity in the channel). In other studies, particle image velocimetry (PIV) has been used to investigate the velocity profile, but as there will be boiling in the flow channel, it cannot be used in this case. Because the beginning of the transient is more interesting and there are events happening faster than during the rest of the case, two different measurement frequencies should be used. For example, in the transient

phase measurements can be made 50 times per second, and when the transient is over only once in a second or two. This way, there is high fidelity data from the initial transient, which is the most important part of the experiment to analyze. During the rest of the experiment, measurements are not needed that frequently, so the size of the data file remains manageable.

The measurement section of the current test facility is 1,7 m tall and the whole channel is 2,7 m tall. The real section of the pressure vessel that the facility is representing is about 7 m tall. To take vertical phenomena into account better, it could be desirable to increase the height of the test facility to more realistic lengths. With suitable support structures, this is achievable.

The test facility presented in this chapter will be dismantled and the measurement section will be placed in storage in the late 2018, as the space in the LUT laboratory is needed for newer experiment equipment. If measurements with this facility are desired, it must be reassembled again. That would open possibilities for larger changes in its structure.

7 PROPOSED TEST PROGRAM AND ARRANGEMENTS

Different sized blocks of insulation materials will be inserted to the test facility to test their properties. The easiest way to attach them to the wall will be by magnets, as has been done in other experiments. This can be done through the windows in the sides of the test facility. Magnets need to be installed inside the insulation blocks. This may cause some errors in the measurements, as the thermal properties of the magnets will not be the same as those of the insulation material itself. However, as the magnetic attachment is one of the best attachment choices for the real insulation, the measurements could be more realistic this way. In addition, it also means that the insulation cannot be arbitrarily thin. The temperatures inside the wall will be measured using the system that is installed.

Constant flow rate is used in experiments. It is achieved by controlling the pump speed and valve positions during the experiment, as the rising water level causes hydrostatic pressure and a need for the pump to operate at higher speed. In a real life accident, the water would rise at a speed of about 8 cm/s. This rate would correspond to about 2,4 l/s flow in the test facility. Different flow speeds should be used in the measurements to provide reasonable estimates for different cases. (Merisaari 2008, 37.)

Temperature of the wall will be around 260 °C and the water about 35 °C for measurements related to the inadvertent initiation of emergency cooling system type of accident. Different temperatures can also be used to test different scenarios. (Merisaari 2008, 37.)

The measured temperatures will be analyzed using the methods and programs described in the chapter 4. Final results will be complete temperature distribution and heat flux from the wall.

8 SIMULATED TEST CASE

To demonstrate the analysis procedure, test cases are simulated by calculating the temperature profile in the test facility steel bar. From these profiles, temperatures in the points where the actual thermocouples would be are used to simulate the measurements. These simulated temperature measurements are then used to calculate heat flux in the wall using ICHP Solver LUT –program in the same way as the real measured temperature data would be. The calculations are made for uninsulated wall and insulated cases to demonstrate the difference.

A 1-D temperature profile for the highest measurement level (thermocouples T120, T126, T130, T134, T109 and T113) in each case is calculated using a defined heat transfer coefficient. The coefficient is changed in discrete time steps, so that during the first minute of the transient, it goes from 13000 W/m^{2}K to 3000 W/m^{2}K, where it will stay for the rest of the calculation, as presented in table 1. The values and the times of their introduction are chosen so that they approximate the measured values obtained during the previous experiments conducted in Lappeenranta University of Technology. The same values are used for all insulated and uninsulated cases. Water cooling the wall is assumed to be in a constant 37 °C temperature. 0,25 second time step is used.

Table 1: Heat transfer coefficient and time steps of their introduction.

Time s	h W/m^{2}K
0	13000
3	11000
9	9000
15	7000
25	5000
60	3000

Three cases were simulated. In the first case there is no insulation. In the second case the insulation is 5 mm of AISI316 steel and in the third case there is 5 mm of MACOR. Material properties are assumed to be constant, and they are presented in Appendix I for the insulators and Appendix II for the pressure vessel. Calculated temperature profiles are presented in figures 12-14. Figures 15-17 show comparison of the calculated temperature profiles at 10, 26 and 61 seconds. These figures show the effect of the insulation well.

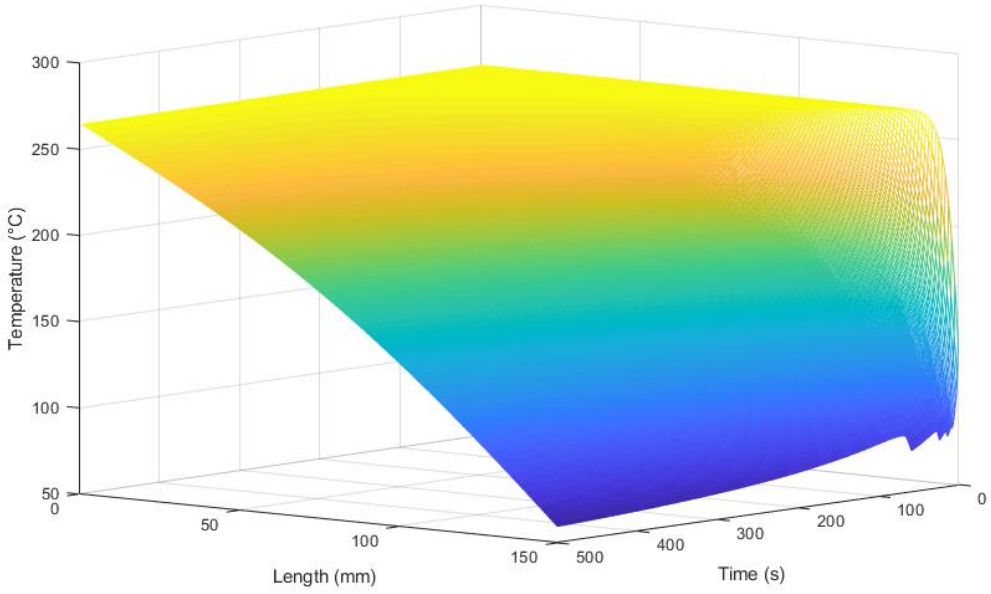

Figure 12: Temperature profile for the uninsulated case.

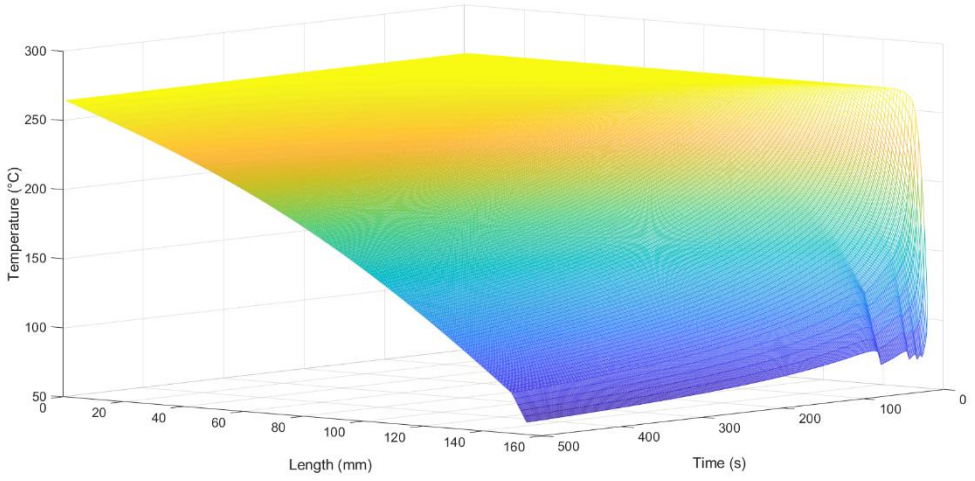

Figure 13: Temperature profile for AISI316 insulation.

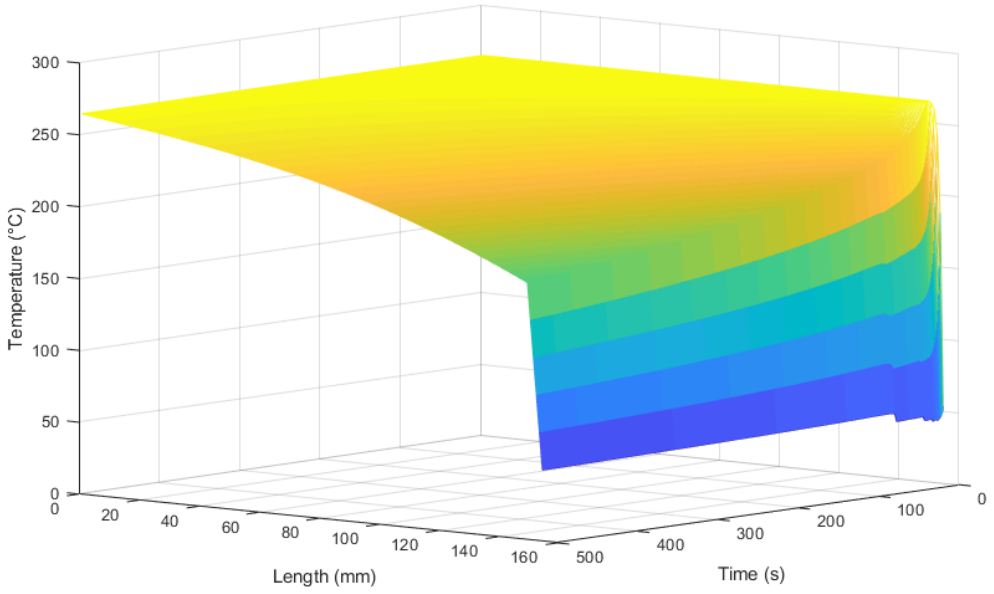

Figure 14: Temperature profile for MACOR insulation.

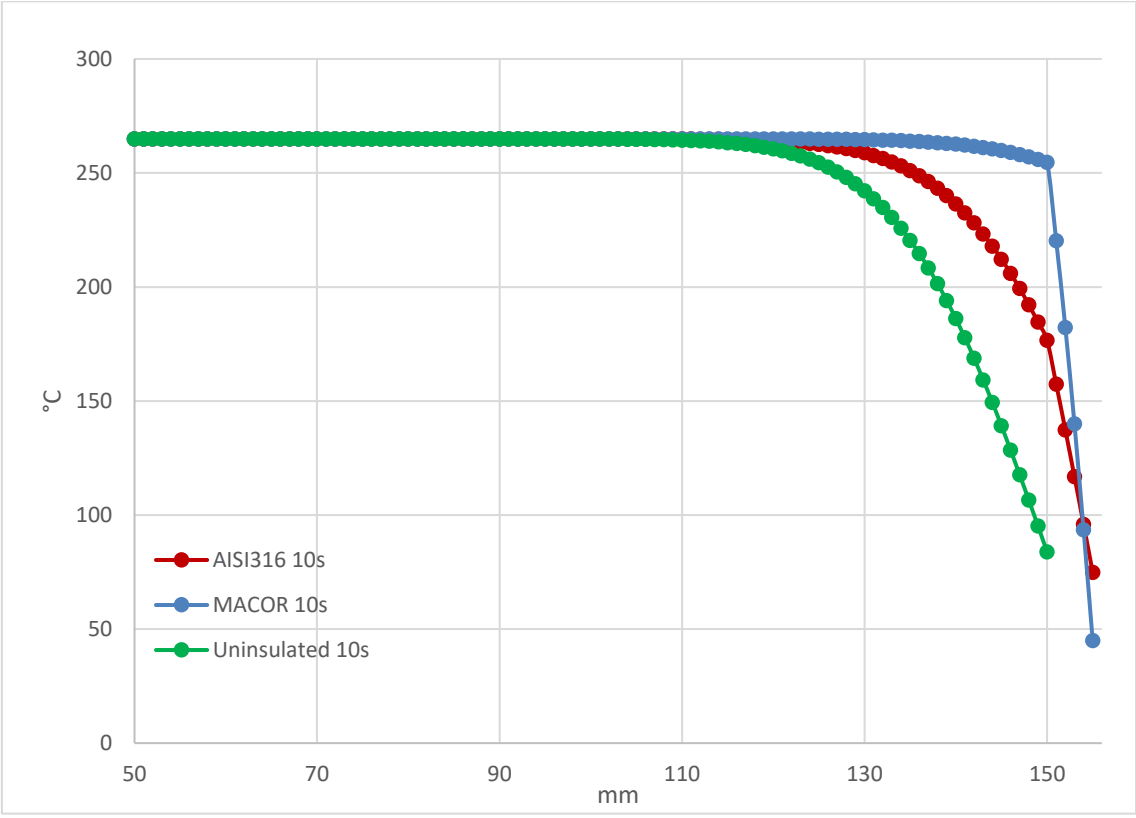

Figure 15: Comparison of temperature profiles at 10 seconds.

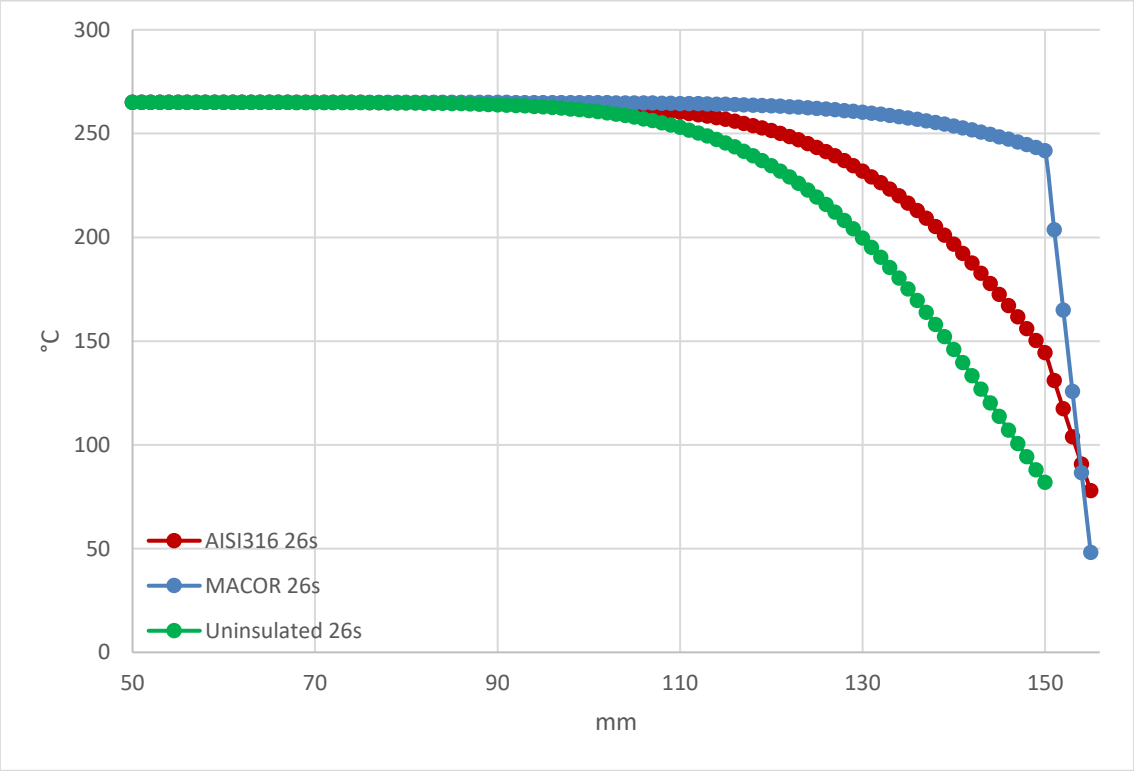

Figure 16: Comparison of temperature profiles at 26 seconds.

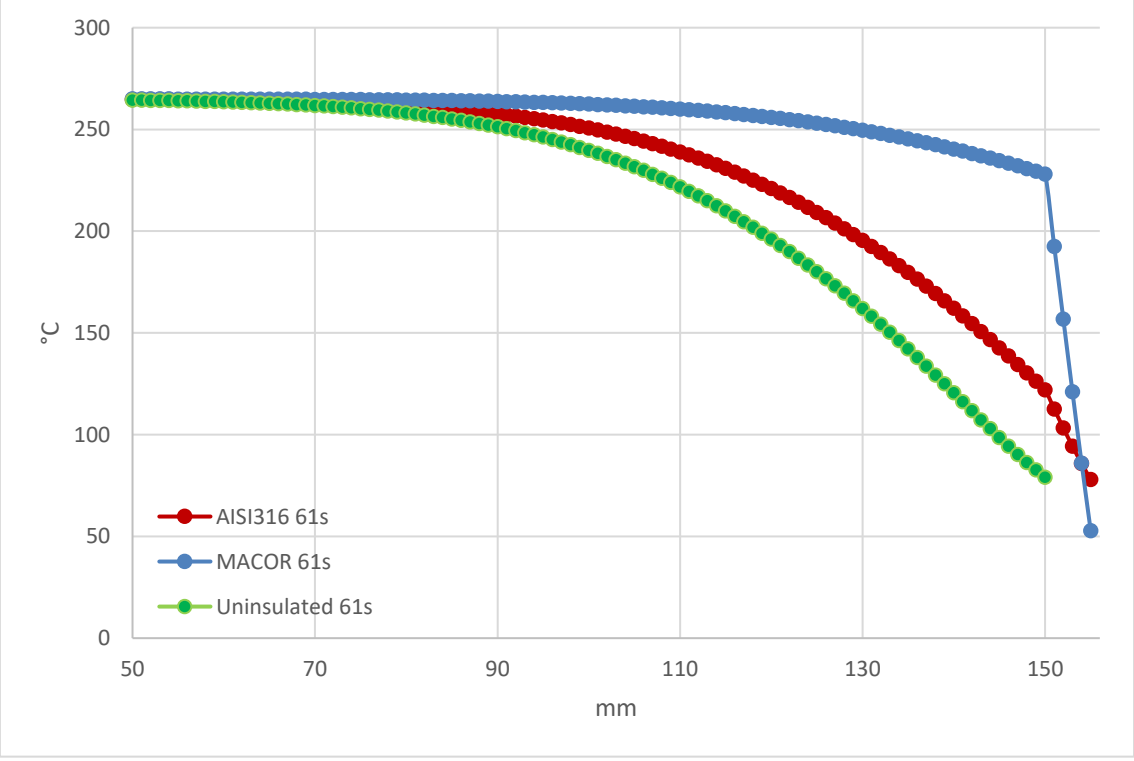

Figure 17: Comparison of temperature profiles at 61 seconds.

The discontinuities in the profiles are due to discretely changing heat transfer coefficient. These temperature profiles are used in the IHCP Solver to calculate the desired heat fluxes. Calculation is done so, that the program takes into account temperature values up to 3 seconds (12 timesteps) forward from the current time step. Heat fluxes from the wall are presented in figures 18-20 and they are compared in figure 21. Comparison of the IHCP calculated heat flux to the heat flux calculated directly from the input temperature data in the uninsulated case is in figures 22 and 23. (Hovi 2018.)

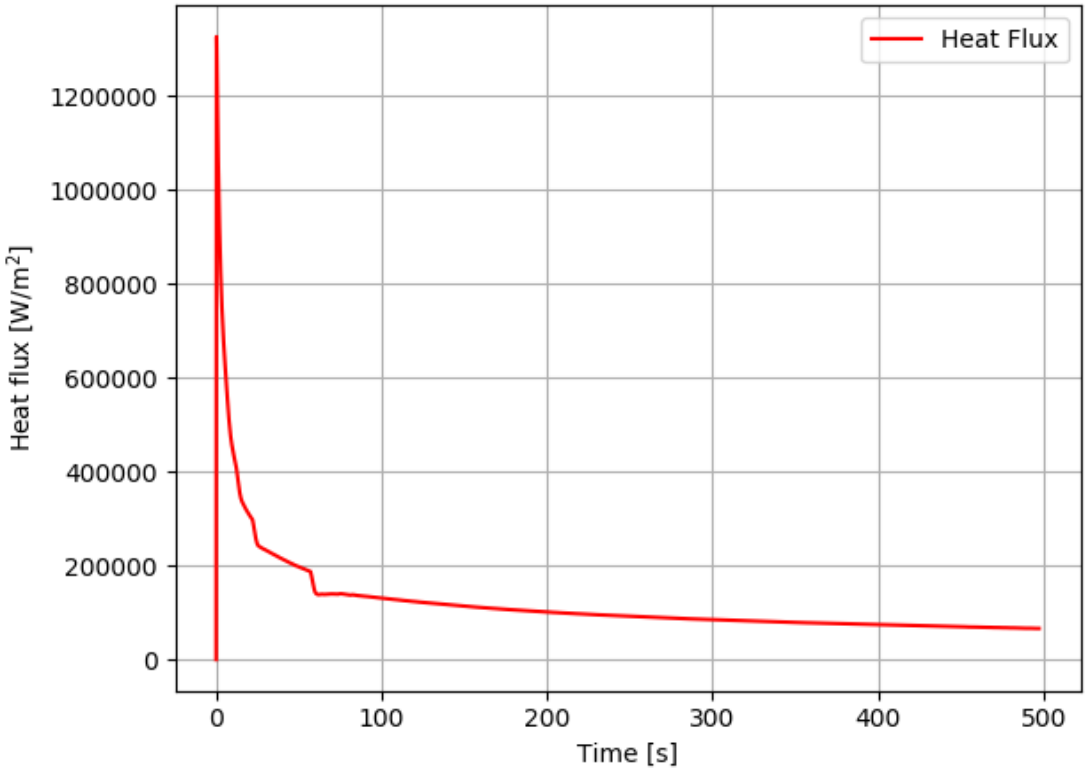

Figure 18: Heat flux without insulation. (Hovi 2018.)

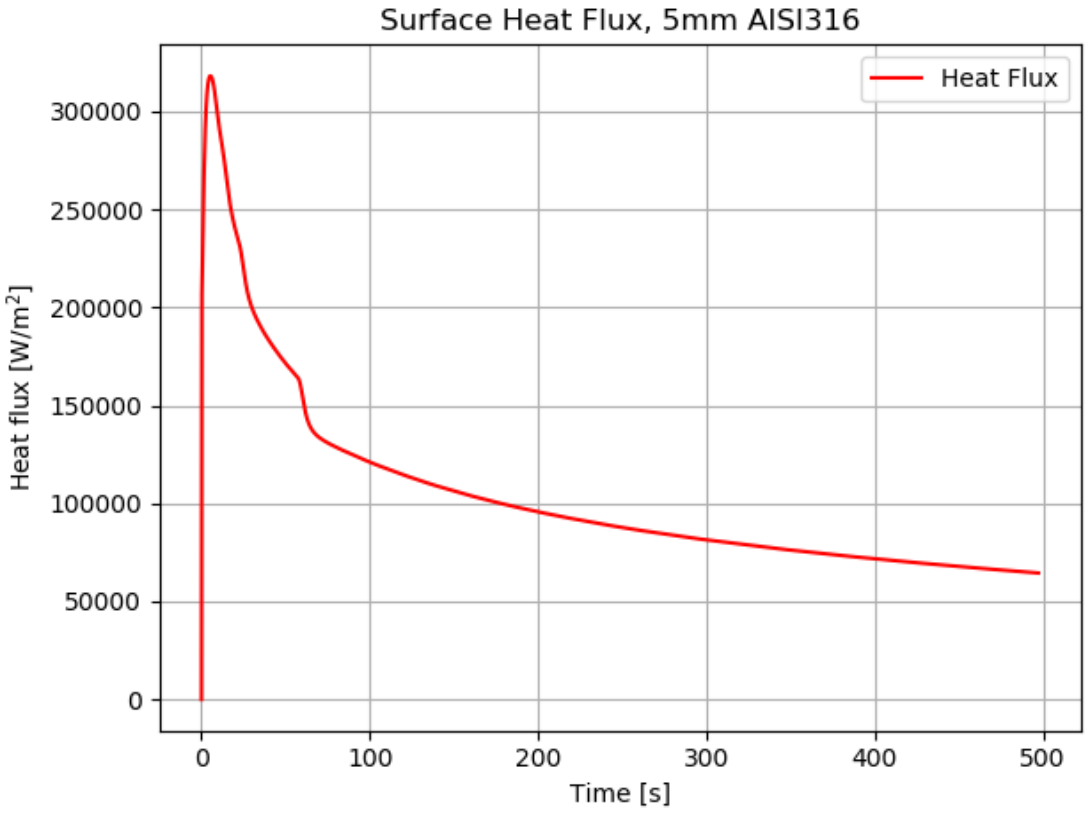

Figure 19: Heat flux with 5 mm of AISI316. (Hovi 2018.)

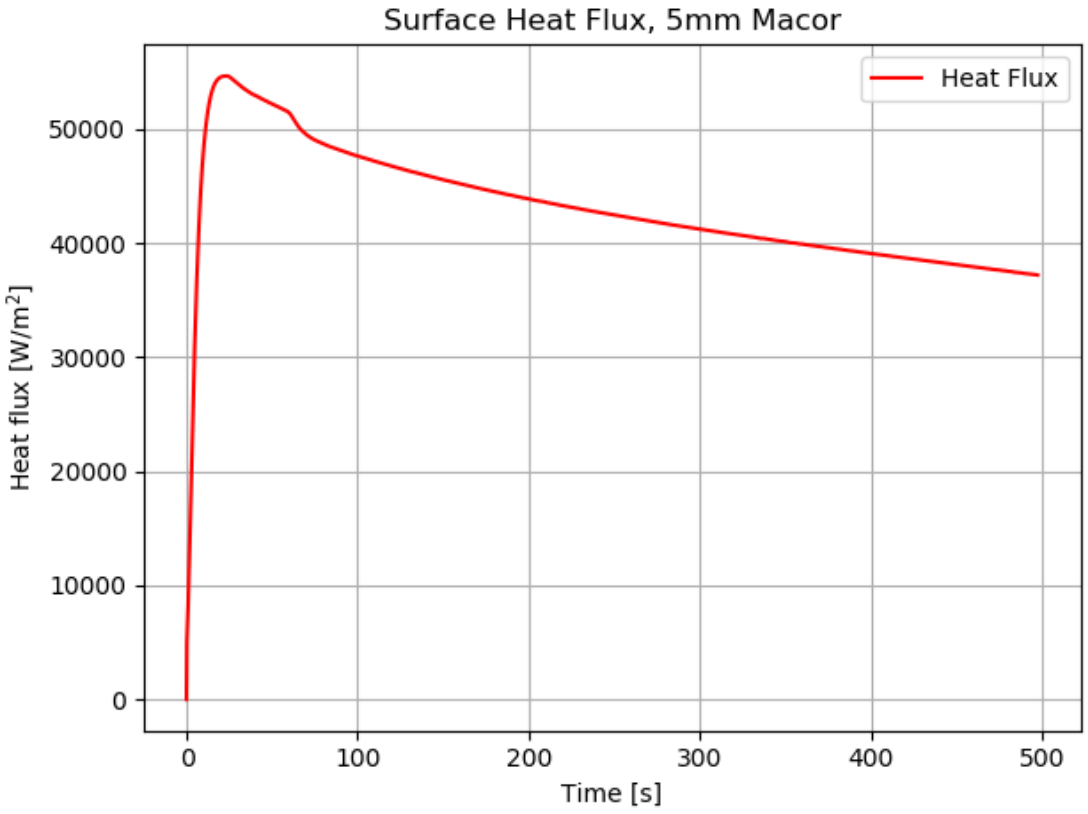

Figure 20: Heat flux with 5 mm of MACOR. (Hovi 2018.)

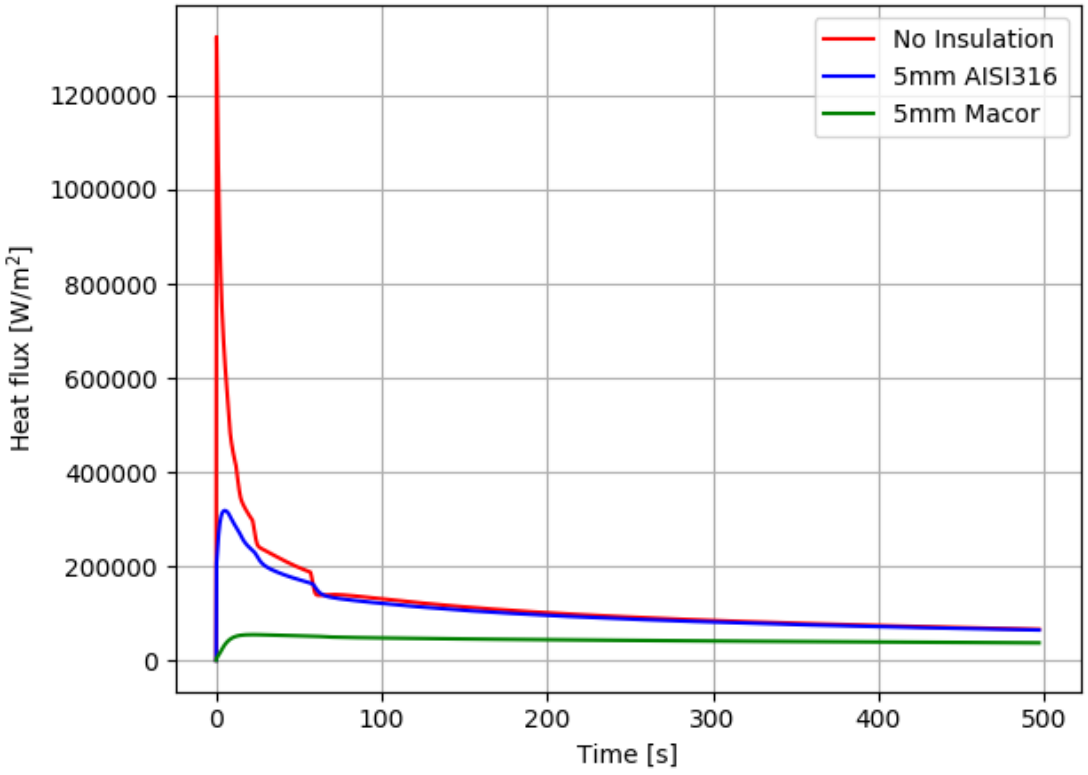

Figure 21: Comparison of the heat fluxes with different insulators. (Hovi 2018.)

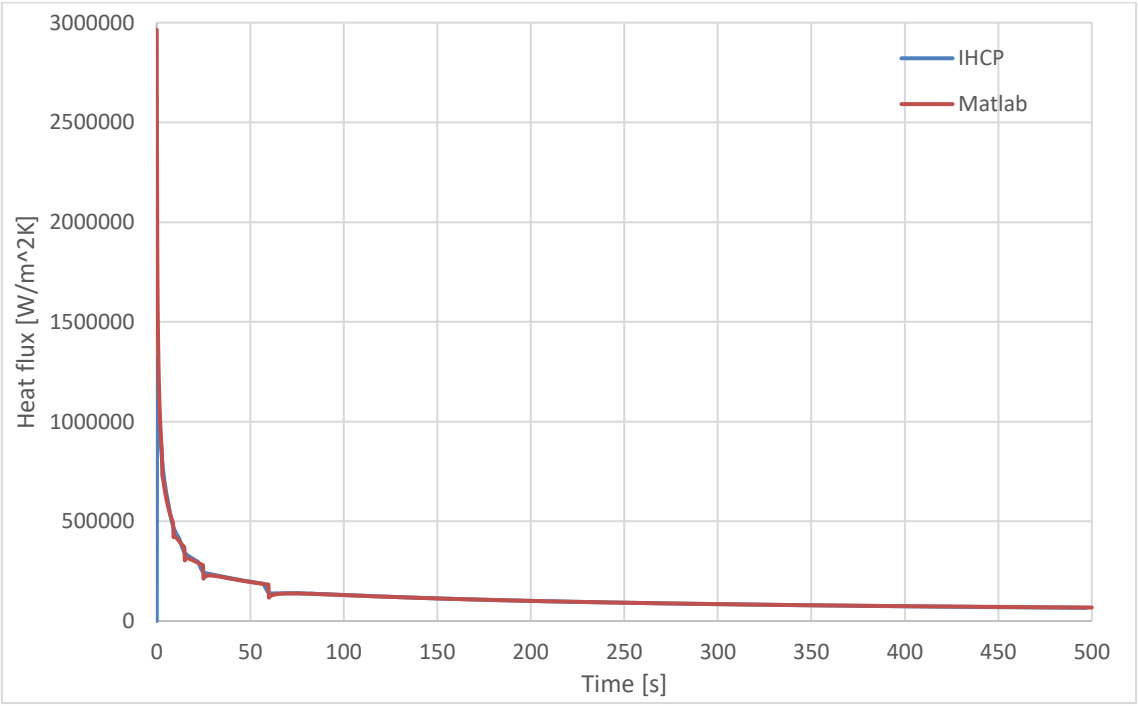

Figure 22: Comparison of heat fluxes in the uninsulated case. Blue line is the heat flux calculated by IHCP and the red one is calculated directly from the temperature data.

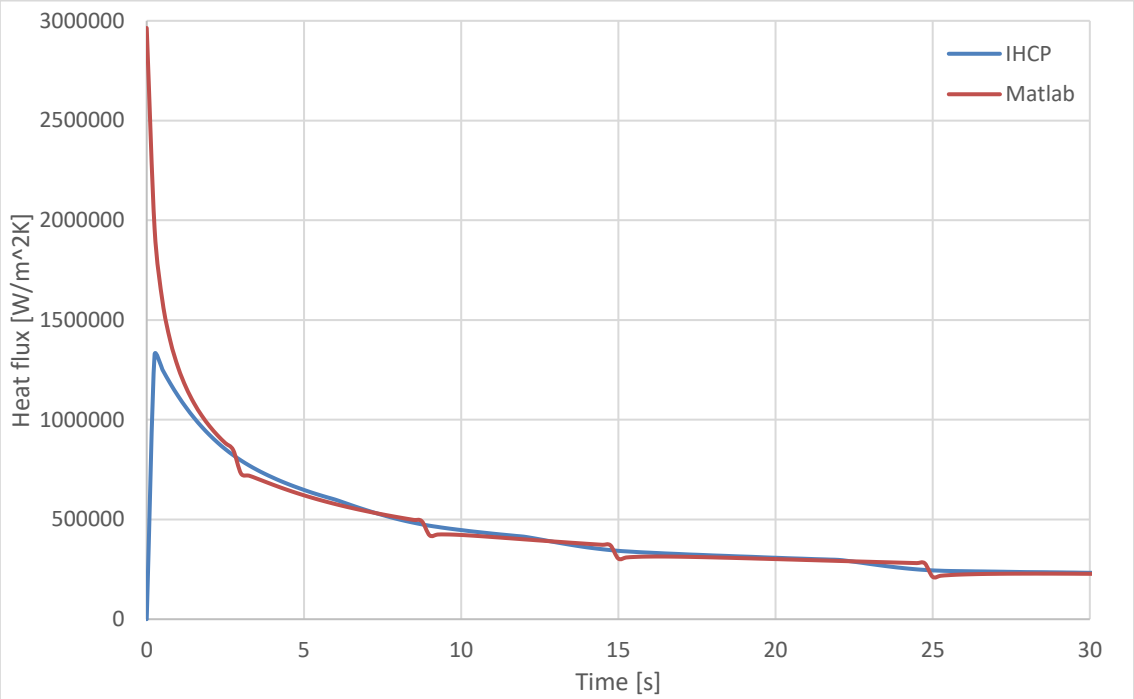

Figure 23: The same comparison as in figure 21, except zoomed to the first 30 seconds to show the difference better.

The figures show, that adding insulation lowers the heat flux greatly. With MACOR-insulation, the heat flux spike in the beginning of the transient is smaller than the heat flux minutes after the start of the transient in uninsulated case. The discontinuity points of the figures correspond to time steps, where the heat transfer coefficient is changed. In the real life, because the coefficient changes gradually, there would not be that kind of points. When comparing the IHCP heat flux to the heat flux calculated directly from the input temperature data, the results are nearly identical after the initial transient. The IHCP calculates the initial transient heat flux spike to be much smaller because the calculation is done using data from multiple timesteps, which flattens rapid changes. This is done, because the real experiments the data would be much noisier due to different measurement errors and other uncertainties, so data from multiple timesteps are needed for mathematical stability.

The purpose of these calculated heat fluxes is to show how the measurement data can be converted to meaningful information. If these were the real measurements, these temperature profiles and heat fluxes could then be used to assess the superiority of different insulation materials. The best insulator is the one that dampens the heat flux

(and therefore the temperature gradient inside the wall) within other parameters discussed previously.

9 DISCUSSION AND CONCLUSIONS

As pressurized thermal shock can lead to very severe accidents, it is an important scenario to study. Many studies about internal overcooling have been made during last decades, but external cases are not as extensively studied. As these accident scenarios involve very rapidly changing heat transfer conditions, experiments are the most reliable way to study them.

One way to relieve the stresses caused by pressurized thermal shock is thermal insulation. It is neither necessary nor desirable to insulate the whole pressure vessel, but the most vulnerable weld seam could possibly be insulated. Many different materials have been considered in the past, and some have been rejected, because they cannot handle the demanding conditions that exist in the reactor cavity. There are, however, some materials that could be used, and experiments should be made to test their properties in real life. One remaining problem is how the insulation elements could be attached to the pressure vessel. The vessel cannot be damaged, so welding or screwing cannot be used. The reactor cavity is also a very cramped space, with only 30 cm gap between the pressure vessel and the surrounding wall. It is also accessible only through small inspection hatches below the RPV. Therefore, the insulator itself must be small and no bulky tools can be used during installation. For these reasons, magnets are probably the most promising way of attachment.

Measurements are necessary to get data for future integrity analyses. The temperature distribution inside the pressure vessel wall and heat flux out of it are the most important parameters. As the heat flux cannot be directly measured, inverse calculation methods must be used to solve it from the measured temperatures. LUT already has the necessary computational tools for this purpose, and that was demonstrated using simulated test data.

REFERENCES

AK Steel. 2008. 316/316L Stainless Steel Data Sheet. West Chester: AK Steel Corporation.

ASM Inc. Titanium Ti-6Al-4V (Grade 5), Annealed. ASM Aerospace Specifications Metals Inc. [online] Available: http://asm.matweb.com/search/SpecificMaterial.asp?bassnum=MTP641 [Accessed 31.10.2018]

Beck, J. V.; Blackwell, B.; St. Clair, C. R. jr. 1985. Inverse Heat Conduction: Ill-posed Problems. New York: Wiley.

Boyd, C. 2008. Pressurized Thermal Shock, PTS. Thicket 2008 conference proceedings, session IX, paper 29. Italy.

Carter, C. B. & Norton, M. G. 2013. Ceramic Materials: Science and Engineering. 2nd ed. New York, NY: Springer New York. ISBN 978-1-4614-3523-5 (eBook).

Corning Inc. MACOR® Data sheet. Corning, New York: Corninc Inc.

The Ceramic Society of Japan. 2012. Advanced Ceramic Technologies & Products. Tokyo: Springer Japan. ISBN 978-4-431-54108-0 (eBook).

Chen, J. C. 1966. A Correlation for Boiling Heat Transfer to Saturated Fluids in Convective Flow. Industrial and Engineering Chemistry, Process Design and Development.

Cheverton, R. D. 1982. Brief account of the effect of overcooling accidents on the integrity of PWR pressure vessels (CONF-820321--25). Oak Ridge National Laboratory, USA.

Churchill, S. W.;Chu, H. H. S. 1975. Correlating Equations for Laminar and Turbulent Free Convection From a Vertical Plate. International Journal of Heat and Mass Transfer. Vol. 18, pp. 1323-1329.

Engineering ToolBox, 2005. Insulation Materials - Temperature Ranges. [online] Available: https://www.engineeringtoolbox.com/insulation-temperatures-d_922.html [Accessed 3.7.2018]

Hovi, T. 2017. Mitigation of external pressurized thermal shock in nuclear reactor pressure vessel. Master's thesis. Lappeenranta University of Technology, School of Energy Systems.

Hovi, T. 2018. Conversation with Tatu Hovi in Lappeenranta University of Technology.

IAEA. 1992. Reactor Pressure Vessel Embrittlement. Vienna: International Atomic Energy Agency. IAEA-TECDOC-659. ISSN 1011-4289.

IAEA. 2006. Guidelines on Pressurized Thermal Shock Analysis for WWER Nuclear Power Plants. 1st Revision. Vienna: International Atomic Energy Agency. IAEA-EBP-WWER-08(Rev. 1). ISSN 1025–2762.

IAEA. 2009. Integrity of Reactor Pressure Vessels in Nuclear Power Plants: Assessment of Irradiation Embrittlement Effects in Reactor Pressure Vessel Steels. Vienna: International Atomic Energy Agency. IAEA Nuclear energy series No. NP-T-3.11. ISBN 978-92-0-101709-3.

IAEA. 2010. Pressurized Thermal Shock in Nuclear Power Plants: Good Practices for Assessment. Deterministic Evaluation for the Integrity of Reactor Pressure Vessel. Vienna: International Atomic Energy Agency. IAEA-TECDOC-1627. ISBN 978-92-0-111109-8.

Incropera, F. P.; DeWitt, D. P.; Bergman, T. L.; Lavine, A. S. 2007. Fundamentals of heat and mass transfer. 6th ed. Hoboken (NJ): Wiley. ISBN 978-0-471-45728-2.

Junninen, P. 2011a. Loviisa 1, PTS, Termohydrauliikkaketjujen valinta reaktoripainesäiliön deterministä turvallisuusanalyysia varten. Fortum internal document. ID: LO1-K311-001-00348.

Junninen, P. 2011b. Loviisa 1 ja 2, PTS, Suojarakennuksen TQ-ruiskutuksen virheellinen käynnistyminen. Fortum internal document. ID: LO1-K311-001-00345.

Krishnan, M.; D. G. R. Sharma. 1996. Determination of the interfacial heat transfer coefficient h in unidirectional heat flow by Beck's non-linear estimation procedure. International Communications in Heat and Mass Transfer, Vol. 23(2), pp. 203-214.

Kolbe, R. & Gahan, E. 1982. Survey of Insulation Used in Nuclear Power Plants and the Potential for Debris Generation. United States. NUREG/CR--2403-Suppl. 1.

Laine, J. 2018. Conversation with Jani Laine in Lappeenranta University of Technology.

Lucefin Group. 2008. 10CrMo9-10. [online] Available: http://www.lucefin.com/wp-content/files_mf/0410crmo91023.pdf [Accessed 31.10.2018]

Merisaari, T. 2008. Heat Transfer Experiments for External Cooling of a Nuclear Reactor Pressure Vessel. Master’s thesis. Lappeenranta University of Technology, Department of Energy and Environmental Engineering.

Murani, J. 1997. Safety measure S 05 'Sump clogging risk'. Mochovce NPP safety improvement and completion. Slovakia: Power Equipment Research Institute.

Myllymäki, K. 2008. Lämmönsiirtokertoimen kokeellinen sovite paineastian ulkopuoliselle jäähdytykselle. Fortumin internal document. ID: FNS-TERMO-125.

National Aeronautics and Space Administration. 1970. Nuclear and Space Radiation Effects on Materials. NASA SP-8053.

Neuvonen, A. 2002. Loviisa 1, Reaktoripainesäiliön PTS-lujuuslaskennan lähtötiedot. Fortum internal document. ID: NUCL-1032.

Papavinasam, S. 2013. Corrosion control in the oil and gas industry. Burlington: Elsevier Science. ISBN: 978-0-12-397022-0.

Promat. 2014. Calcium Silicate Insulation. Tisselt: Promat International N.V.

Scagliusi, S. R.; Cardoso, E. C. L.; Lugão, A. B. 2015. Gamma-radiation Effect on Thermal Ageing of Butyl Rubber Compounds. São Paulo: 2015 International Nuclear Atlantic Conference. ISBN: 978-85-99141-06-9.

Toppila, T. & Launiainen, S. 2018. Conversation with Toppila and Launiainen in Fortum, Espoo.

Tuomisto, Harri. 1997. Overcooling Transient Selection and Thermal Hydraulic Analyses of the Loviisa PTS Assessments. International Atomic Energy Agency. IWG-LMNPP--96/1.

Žemulis, G. 2017. PTS-analyysien tulosten katselmointi. Fortum internal document.

APPENDIX I: THERMAL PROPERTIES OF SOME POSSIBLE INSULATION MATERIALS

Material thicknesses are the same as those used in *Mitigation of external pressurized thermal shock in nuclear reactor pressure vessel*. Convective heat transfer coefficient used to calculate Biot numbers is 8000 W/m^2K. Characteristic time for Fourier number (3 seconds) is an approximation from previous measurements made in the LUT.

MACOR® (Corning Inc.)

Density	ρ	2520	kg/m^3	
Specific Heat, 25 °C	c_p	790	J/kgK	
Thermal Conductivity, 25 °C	k	1,46	W/mK	
Thermal Diffusivity, 25 °C	α	$7{,}30 \cdot 10^{-7}$	m^2/s	
Continous Operating Temperature		800	°C	
Maximum No load Temperature		1000	°C	
Thickness (mm)	3	5	10	20
Bi	16	27	55	110
Fo(3 s)	0,243	0,0876	0,0219	0,00548

Calcium silicate (PROMATECT-H) (Promat 2014.)

Bulk density	ρ	870	kg/m^3
Specific Heat, 400 °C	c_p	920	J/kgK
Thermal Conductivity, 200 °C mean	k	0,21	W/mK
Thermal Diffusivity	α	$2{,}62 \cdot 10^{-7}$	m^2/s
Classification temperature		400	°C
Thickness (mm)	3	5	10
Bi	114	190	381
Fo (3 s)	0,0874	0,0315	0,00197

Stainless steel AISI316 (AK Steel 2008.)

Density	ρ	7990	kg/m^3	
Specific Heat, 0-100 °C	c_p	500	J/kgK	
Thermal Conductivity, 100 °C	k	16,2	W/mK	
Thermal Diffusivity	α	$4{,}06 \cdot 10^{-6}$	m^2/s	
Melting Range		1371-1399	°C	
Thickness (mm)	5	10	20	30
Bi	2,47	4,94	9,88	14,8
Fo (3 s)	0,487	0,122	0,0304	0,0135

Titanium Ti-6Al-4V (ASM Inc.)

Density	ρ	4430	kg/m^3	
Specific Heat	c_p	526	J/kgK	
Thermal Conductivity	k	6,7	W/mK	
Thermal Diffusivity	α	$2{,}88 \cdot 10^{-6}$	m^2/s	
Melting Point		1604-1660	°C	
Thickness (mm)	5	10	20	30
Bi	5,97	11,9	23,9	35,8
Fo (3 s)	0,345	0,0863	0,0216	0,00958

Zirconium (Incropera et al. 2007, 932.)

Density	ρ	7140	kg/m^3	
Specific Heat, 27 °C	c_p	278	J/kgK	
Thermal Conductivity, 27 °C	k	22,7	W/mK	
Thermal Diffusivity, 27 °C	α	$1{,}14 \cdot 10^{-5}$	m^2/s	
Melting Point		2125	K	
Thickness (mm)	5	10	20	30
Bi	1,76	3,52	7,05	10,6
Fo (3 s)	1,37	0,343	0,0858	0,0381

10CrMo9-10 –steel (Lucefin Group 2008.)

Density	ρ	7840	kg/m^3	
Specific Heat, 100 °C	c_p	479	J/kgK	
Thermal Conductivity, 100 °C	k	37,3	W/mK	
Thermal Diffusivity, 100 °C	α	$9{,}93 \cdot 10^{-5}$	m^2/s	
Melting Point		1100+	°C	
Thickness (mm)	5	10	20	30
Bi	1,07	2,14	4,29	6,43
Fo (3 s)	1,19	0,298	0,0745	0,0331

APPENDIX II: THERMAL PROPERTIES OF THE REACTOR PRESSURE VESSEL WALL

(Neuvonen 2002, 2.)

Density	ρ	7800	kg/m^3
Specific Heat, 100 °C	c_p	502	J/kgK
Thermal Conductivity, 100 °C	k	39,8	W/mK
Thermal Diffusivity, 100 °C	α	$1{,}02 \cdot 10^{-5}$	m^2/s

Thickness (mm)	150
Fo (3 s)	0,00136
Bi (8000 W/m^2K)	30,2
Bi (4000 W/m^2K)	15,1
Bi (2000 W/m^2K)	7,5
Bi (1000 W/m^2K)	3,8

APPENDIX III: MEASUREMENT INSTRUMENTATION

Code	Measurement	Measurement device	Measurement range	Error estimation
T101	Temperature in the flow channel	Thermocouple K-type, NiCrNi, ∅3.0	0–200 °C	± 2 °C
T102	Temperature in the flow channel	Thermocouple K-type, NiCrNi, ∅3.0	0–200 °C	± 2 °C
T103	Temperature in the flow channel	Thermocouple K-type, NiCrNi, ∅3.0	0–200 °C	± 2 °C
T104	Temperature in the flow channel	Thermocouple K-type, NiCrNi, ∅3.0	0–200 °C	± 2 °C
T105	Temperature in the flow channel	Thermocouple K-type, NiCrNi, ∅3.0	0–200 °C	± 2 °C
T106	Temperature in the steel bar	Thermocouple K-type, NiCrNi, ∅3.0	0–200 °C	± 2 °C
T107	Temperature in the steel bar	Thermocouple K-type, NiCrNi, ∅3.0	0–200 °C	± 2 °C
T108	Temperature in the steel bar	Thermocouple K-type, NiCrNi, ∅3.0	0–200 °C	± 2 °C
T109	Temperature in the steel bar	Thermocouple K-type, NiCrNi, ∅3.0	0–200 °C	± 2 °C
T110	Temperature in the steel bar	Thermocouple K-type, NiCrNi, ∅3.0	0–200 °C	± 2 °C
T111	Temperature in the steel bar	Thermocouple K-type, NiCrNi, ∅3.0	0–200 °C	± 2 °C
T112	Temperature in the steel bar	Thermocouple K-type, NiCrNi, ∅3.0	0–200 °C	± 2 °C
T113	Temperature in the steel bar	Thermocouple K-type, NiCrNi, ∅3.0	0–200 °C	± 2 °C
T114	Temperature in the steel bar	Thermocouple K-type, NiCrNi, ∅3.0	0–200 °C	± 2 °C
T115	Temperature in the steel bar	Thermocouple K-type, NiCrNi, ∅3.0	0–200 °C	± 2 °C
T117	Temperature in the steel bar surface	Thermocouple K-type, NiCrNi, ∅1.0	0–200 °C	± 2 °C
T118	Temperature in the steel bar surface	Thermocouple K-type, NiCrNi, ∅1.0	0–200 °C	± 2 °C
T119	Temperature in the steel bar surface	Thermocouple K-type, NiCrNi, ∅1.0	0–200 °C	± 2 °C
T120	Temperature in the steel bar surface	Thermocouple K-type, NiCrNi, ∅1.0	0–200 °C	± 2 °C
T121	Temperature in the flow channel	Thermocouple K-type, NiCrNi, ∅3.0	0–200 °C	± 2 °C
T122	Temperature in the flow channel	Thermocouple K-type, NiCrNi, ∅3.0	0–200 °C	± 2 °C

T123	Temperature in the steel bar	Thermocouple K-type, NiCrNi, ∅1.0/3.0	0–200 °C	± 2 °C
T124	Temperature in the steel bar	Thermocouple K-type, NiCrNi, ∅1.0/3.0	0–200 °C	± 2 °C
T125	Temperature in the steel bar	Thermocouple K-type, NiCrNi, ∅1.0/3.0	0–200 °C	± 2 °C
T126	Temperature in the steel bar	Thermocouple K-type, NiCrNi, ∅1.0/3.0	0–200 °C	± 2 °C
T127	Temperature in the steel bar	Thermocouple K-type, NiCrNi, ∅1.0/3.0	0–200 °C	± 2 °C
T128	Temperature in the steel bar	Thermocouple K-type, NiCrNi, ∅1.0/3.0	0–200 °C	± 2 °C
T129	Temperature in the steel bar	Thermocouple K-type, NiCrNi, ∅1.0/3.0	0–200 °C	± 2 °C
T130	Temperature in the steel bar	Thermocouple K-type, NiCrNi, ∅1.0/3.0	0–200 °C	± 2 °C
T131	Temperature in the steel bar	Thermocouple K-type, NiCrNi, ∅1.0/3.0	0–200 °C	± 2 °C
T132	Temperature in the steel bar	Thermocouple K-type, NiCrNi, ∅1.0/3.0	0–200 °C	± 2 °C
T133	Temperature in the steel bar	Thermocouple K-type, NiCrNi, ∅1.0/3.0	0–200 °C	± 2 °C
T134	Temperature in the steel bar	Thermocouple K-type, NiCrNi, ∅1.0/3.0	0–200 °C	± 2 °C
D201	Pressure difference over the mock-up	Pressure-difference transmitter Foxboro IDP50	0–35 kPa	± 26 Pa
D205	Pressure difference over the pump 1	Pressure-difference transmitter Foxboro IDP10	0–20 bar	± 0.025 bar
D206	Pressure difference over the pump 3	Pressure-difference transmitter Foxboro IDP10	0–20 bar	± 0.025 bar
T206	Temperature in the steel bar	Thermocouple K-type, NiCrNi, ∅3.0	0–200 °C	± 2 °C
T209	Temperature in the steel bar	Thermocouple K-type, NiCrNi, ∅3.0	0–200 °C	± 2 °C
T231	Temperature in the steel bar	Thermocouple K-type, NiCrNi, ∅1.0/3.0	0–200 °C	± 2 °C
T234	Temperature in the steel bar	Thermocouple K-type, NiCrNi, ∅1.0/3.0	0–200 °C	± 2 °C
F300	Flow rate in the flow channel	Magnetic flowmeter Krohne Altometer Optiflux 4000	0–55 l/s	± 0.165 l/s
F302	Flow rate in the auxiliary loop	Magnetic flowmeter Foxboro 8006A-WCR	0–150 l/s	± 0.495 l/s
L400	Water level in the tank 1	Magnetostrictive level	0–3000 mm	± 2.77 mm

		transmitter K-Tek AT100		
T500	Gas temperature in the tank 1	Resistance temperature detector ∅3.0	0–200 °C	± 1 °C
T501	Water temperature in the tank 1	Resistance temperature detector ∅3.0	0–200 °C	± 1 °C
T510	Temperature in the cooling loop	Thermocouple K-tyyppi, NiCrNi, ∅1.5	0–200 °C	± 2 °C
T511	Temperature in the auxiliary loop	Resistance temperature detector ∅3.0	0–200 °C	± 1 °C
T512	Temperature in the auxiliary loop	Resistance temperature detector ∅3.0	0–200 °C	± 1 °C
T513	Gas temperature in the tank 2	Resistance temperature detector ∅3.0	0–200 °C	± 1 °C
T514	Water temperature in the tank 2	Resistance temperature detector ∅3.0	0–200 °C	± 1 °C
T515	Ambient temperature	Resistance temperature detector ∅3.0	0–200 °C	± 1 °C
T520	Temperature in the auxiliary loop	Resistance temperature detector ∅3.0	0–200 °C	± 1 °C